EDGE STRESSES IN A COMPOSITE PLATE WITH A HOLE — A HYBRID FEM APPROACH

A Thesis Submitted
in Partial Fulfilment of the Requirements
for the Degree of

MASTER OF TECHNOLOGY

by

MAKARAND JOSHI

to the

DEPARTMENT OF MECHANICAL ENGINEERING

INDIAN INSTITUTE OF TECHNOLOGY KANPUR

JULY, 1991

CERTIFICATE

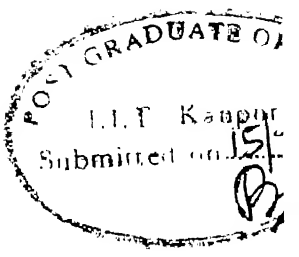

This is to certify that the work entitled "Edge Stresses in a Composite Plate With a Hole - A Singular Hybrid FEM Approach" by Makarand Ganesh Joshi has been carried out under my supervision and has not been submitted elsewhere for a degree.

N. N. KISHORE

Assistant Professor

Department of Mechanical Engineering

Indian Institute of Technology

Kanpur, 208016

ACKNOWLDGEMENTS

I am extremely grateful to Dr. N.N. Kishore for his able guidance, critical appraisals and thought provoking suggestions, from the inception to the completion of this work.

I feel indebted to Vijay Pankhawala, Vinu and Madhav who helped me draw the figures and graphs. I would like to thank all in the ESA lab. who helped me take the rough and the final prints of the thesis. I would also like to thank G.K. Singh and Subrato Saha for the enlightening discussions on this work. A million thanks to the ghat 'Aish'ociation, GK, Shankh, Rajiv, Nachiketa, Kak and all others who made my stay at IIT-K a pleasant and memorable one.

Makarand Joshi

CONTENTS

		PAGE
CERTIFICATE		.. i
ACKNOWLEDGEMENTS		.. ii
CONTENTS		.. iii
LIST OF SYMBOLS		.. v
LIST OF FIGURES		.. vii
SYNOPSIS		.. x
CHAPTER I	INTRODUCTION	
	1.1 Introduction	.. 1
	1.2 Literature Survey	.. 2
	1.3 Scope of present work	.. 6
CHAPTER II	PROBLEM DEFINITION	
	2.1 Introduction	.. 8
	2.2 Problem definition	.. 8
CHAPTER III	THE SINGULAR HYBRID FEM APPROACH APPLIED TO LAMINATED PLATES	
	3.1 Introduction	.. 12
	3.2 Hybrid stress elements	.. 13
	3.3 Layer stress interpolation for non-singular hybrid and singular hybrid elements	.. 22
CHAPTER IV	RESULTS AND DISCUSSIONS	
	4.1 Interlaminar stresses near the circular hole boundary in symmetric composite laminate	.. 39
	4.2 Interlaminar stresses near the square hole boundary in symmetric composite laminate	.. 42

CHAPTER V CONCLUSIONS AND SCOPE FOR FUTURE WORK

5.1 Conclusions .. 67

5.2 Scope for future work .. 67

REFERENCES .. 69

APPENDIX A .. 73

APPENDIX B .. 76

LIST OF SYMBOLS

X_1, X_2, X_3	Material co-ordinate system
x, y, z	Global co-ordinate system
θ	Angle between the material and global co-ordinate systems
σ^i	Vector of stresses in layer i
$\hat{\epsilon}^i$	Vector of strains in layer i
$\underline{u}^i$	Displacement vector for layer i
S^i	Compliance matrix
$\underline{T}^i$	Prescribed tractions
V_{n_i}	Volume of layer i
$S_{\sigma n_i}$	Portion of element boundary on which tractions are prescribed
I	Total number of layers in the laminated composite
E_{11}, E_{22}	Young's moduli in the fibre and transverse directions
ν_{12}, ν_{23}	Major and minor Poisson's ratio respectively
P^i	Matrix of polynomials of stress assumption
$\underline{\beta}^i$	Constants used in stress assumptions
$N_j(\xi, \eta)$	Biquadratic Serendipity shape functions
ξ, η, τ	The normalised co-ordinate system
$\underline{q}^i$	Nodal displacements of layer i
N^i	Shape functions in normalised co-ordinates (ξ,η,τ)
D^i	Strain displacement differential operator matrix

$\|J\|$	Jacobian for co-ordinate transformation
$\bar{t}_i$	Half the thickness of layer i
K	Elemental stiffness matrix
Q	Elemental load vector
C_s^i	Matrix relating layer stress parameters β^i to laminate stress parameters β
C_d^i	Matrix relating nodal displacements q^i to laminate nodal displacements q
λ	Power of singularity
r, θ, z	cylindrical co-ordinates
s,ϕ	polar co-ordinate radius and angle
r_{cg}	Radius of centroid of the sector
r_{cn}	Radius of the mid-node on the boundary of the sector
σ_r	Stress in the radial direction
σ_z	Stress in the axial direction
σ_θ	Stress in the circumferential direction (Hoop stress)
τ_{rz}	Shear stress
ϵ_r	Strain in the radial direction
ϵ_z	Strain in the axial direction
ϵ_θ	Circumferential strain
γ_{rz}	Shear strain

LIST OF FIGURES

FIGURE NO.	TITLE	PAGE
2.1	Geometry of laminete with a circular hole	.. 10
2.2	Geometry of laminate with a square hole	.. 11
3.1	Geometry and layer numbering of multilayer plate element	.. 33
3.2	Lamina with its principal material axes oriented at angle θ with reference to the global axes	.. 34
3.3	Displacement degrees of freedom	.. 35
3.4	Singular elements at hole boundary	.. 36
3.5	Mapping from natural coordinates ξ, η to physical coordinates s and θ	.. 37
3.6	Position of any point on sector w.r.t. axisymmetric axes.	38
4.1	FEM Discretization of laminate plate with circular hole (85 elements)	.. 45
4.2	FEM Discretization of laminate plate with circular hole (170 elements)	.. 46
4.3	Angular variation of power of singularity	.. 47
4.4	σ_z radial distribution for 0/90 laminate with circular hole (85 elements) $\theta = 0^o$	.. 48
4.5	σ_z radial distribution for 0/90 laminate with circular hole (85 elements) $\theta = 45^o$	.. 49
4.6	σ_z radial distribution for 0/90 laminate with circular hole (85 elements) $\theta = 90^o$	.. 50
4.7	σ_z radial distribution for 0/90 laminate with circular	

	hole (170 elements) $\theta = 0^{o}$	.. 51
4.8	σ_z radial distribution for 0/90 laminate with circular hole (170 elements) $\theta = 45^{o}$	.. 52
4.9	σ_z radial distribution for 0/90 laminate with circular hole (170 elements) $\theta = 90^{o}$	.. 53
4.10	τ_{rz} radial distribution for 0/90 laminate with circular hole (170 elements)	.. 54
4.11	σ_θ through thickness distribution for 0/90 laminate with circular hole (170 elements)	.. 55
4.12	σ_z through thickness distribution for 0/90 laminate with circular hole (170 elements)	.. 56
4.13	σ_z radial distribution for 90/0 laminate with circular hole (85 elements)	.. 57
4.14	τ_{rz} radial distribution for 90/0 laminate with circular hole (85 elements)	..58
4.15	σ_θ through thickness distribution for 90/0 laminate with circular hole (85 elements)	.. 59
4.16	σ_z through thickness distribution for 90/0 laminate with circular hole (85 elements)	.. 60
4.17	FEM Discretization of laminate plate with square hole (85 elements)	.. 61
4.18	FEM Discretization of laminate plate with square hole (170 elements)	.. 62
4.19	σ_z radial distribution for 0/90 laminate with square hole (85 elements)	.. 63
4.20	τ_{rz} radial distribution for 0/90 laminate with square hole (170 elements)	.. 64

4.21 σ_θ through thickness distribution for 0/90 laminate with circular hole (85 elements) .. 65

4.22 σ_z through thickness distribution for 0/90 laminate with circular hole (85 elements) .. 66

SYNOPSIS

Composite materials have found wide application in the aerospace and aircraft industry, due to their decisive advantages in terms of structural properties, over the other conventional materials. This has boosted the research on such materials in the past few years, mainly in the areas related to the manufacture, and fracture and fatigue.

Due to the design requirements, the composite laminates may have holes, cut-outs etc. These provide free edges where, a three dimensional state of stress develops even under uniaxial loading. This happens due to the sudden change in the material property at the interface. Delamination is a major cause of failures in composite laminates. The present work, endevours to analyse the edge stresses in symmetric crossply laminates having central circular/square hole, at the hole boundary, which is a potential region for the delamination type of failures.

Many attempts have been made in the past to solve this problem by the application of semi-analytical and finite element methods. The analytical methods are complex in their formulation and solutions, while the displacement based FEM solutions require a very fine mesh and large computing times. Hybrid FEM solutions, which have been developed in the recent past, provide expeditous computation but do not guarantee convergence at the edges of interfaces. The use of singular elements can overcome this drawback. The appropriate singular elements, when used in the regions close to the hole model the singularity of the stresses and improve convergence.

In the present case, a hybrid stress 8-node isoparametric multi-

layered plate element which includes an appropriate singular term has been used. The hybrid stress model is based on the modified complimentary energy principle and takes into account the transverse deformation effects. All the displacements are assumed to vary linearly through the thickness.

The singular element, which is used in the boudary layer region uses the hybrid stress interpolation in conjunction with a singular term. The power of singularity has been found by solving a separate eigen value problem.

A computer code in FORTRAN language has been developed to solve the above problem. The results show significant improvement in the accuracy and efficiency of the present method compared with the earlier methods. Also, they indicate a mixed mode failure near the hole boundary.

CHAPTER 1

INTRODUCTION

1.1 Composite Materials :

Composite materials are made of two or more constituents, which on a macroscale have distinct interface separating them. These materials achieve certain physical properties not realizable in their constituents, such as high specific strength and stiffness, and controlled anisotropy. As they are usually endowed with good fatigue and corrosion resistance, low heat conductivity, good electrical insulation properties, favourable cost effectiveness etc., they find wide applications in aerospace and transport industry. In recent past extensive research work has been carried out on the manufacture, characterization, fatigue and fracture of these materials, to promote further use of these materials.

1.1.1 Interlaminar Stresses/Edge Effects :

A prominent disadvantage of laminated composites is that under simple uniaxial or biaxial loading, they develop a triaxial state of stress near the free edges. These out-of-plane stresses are called the "inter-laminar" stresses and this phenomena is called the edge effect, as it is evident only in the close vicinity of the free edge, in a region approximately equal to the thickness of the laminate. These interlaminar stresses are of critical concern to designers as they may lead to delamination type of failures at loads well below those corresponding to inplane failure. Interlaminar stresses may be present as a result of mechanical, thermal or moisture loading.

These stresses between layers are caused due to the mismatch of properties of bonded adjacent layers and the presence of gradients in the inplane stresses. Stress free boundaries present the most severe stress gradients and hence the most severe interlaminar stresses.

In contrast to the isotropic materials, the anisotropic materials present a very broad range of variation in properties across the adjacent layers. The material properties which result in a mismatch of properties are primarily the Poisson's ratio, the coefficients of mutual influence, and the thermal and hygroscopic expansion coefficients.The transverse shear stresses result in the sliding of adjacent layers over one another. Though this phenomena is localised near the free edges and insignificant in the far field regions, it may prove fatal under fatigue loading as it may lead to matrix cracks. Also, the transverse normal stress may lead to delamination type of failures.

Due to functional or design requirements, the composite may contain holes, cut-outs etc. These, apart from the free edges show stress singularity. Hence the analysis of laminated composites to estimate the interlaminar stresses proves important from the design point of view.

1.2 Literature Survey :

The existence of interlaminar stresses along the free edges, in the boundary layer region of a laminated composites has been known for some time. The first publication dealing with the singular behaviour of stresses at the intersection of a boundary and bonded dissimilar materials is that of Bogy (1968). The earliest work dealing with the anisotropic materials appears to be the study by Puppo and Evenson (1970), in which, the laminate

was modeled as a set of anisotropic layers separated by an isotropic layer of adhesive material having negligible stiffness.

The first complete three-dimensional analysis of interlaminar stresses by applying finite difference technique was done by Pipes and Pagano (1970). They showed that interlaminar stresses existed along the free edge in the boundary layer region and that its width was approximately equal to the laminate thickness. The singular behaviour of the transverse normal stress σ_z and the transverse shear stress τ_{rz} varies to a large extent with laminate configuration (material, fiber orientation, layer thickness and stacking sequence). These results were later experimentally verified by Pipes and Daniels (1971).

The relationship between interlaminar stresses and delamination was analytically disscussed in many subsequent papers. Pagano (1974) presented an approach which accounted for the influence of pertinent material and geometric parameters on the distribution of normal stress σ_z along the central plane of a symmetric finite width composite laminate. Pipes and Pagano (1974) developed an approximate elasticity solution for the response of finite width, symmetric angle-ply laminate under uniform axial strain.

Tang (1976) derived the governing differential equations for uniformly loaded rectangular composite plate using the classical laminate theory and approximate boundary conditions. Tang (1977) later used a boundary layer theory to obtain stress distribution around a circular hole in $[0/90]_S$ and $[\pm 45]_S$ laminates, using very large values for the ratio of hole radius to ply thickness.

Pagano (1978) reduced the free edge class of boundary value problem

to a one-dimensional problem to predict the stress fields. The solution involved consideration of 13N algebraic and ordinary differential equations, where N stands for the number of layers.

Kassapoglous and Lagace (1986) presented a method which predicted interlaminar stress state. The expressions for stresses were in terms of exponentials based on the shape that the interlaminar stress must take in order to ensure overall force and moment equilibrium. Boundary conditions and traction continuity between plies were satisfied exactly.

Chaudhari and Siede (1987) presented an approximate semianalytical method to determine transverse shear stress variation across the thickness. The method utilised a quadratic displacement potential energy based FEM.

A three-dimensional finite differnce model by Altus *et.al.* (1980) followed a finite element formulation by Isakson and Levy (1971) to determine the interlaminar stresses for generalised plane strain conditions based on the work of Pipes and Pagano (1970). Subsequently many results were published using finite element techniques.

Rybicki (1971) presented a three-dimensional FE formulation using complementary energy approach. Wang and Crossman (1977) included mechanical, thermal and hygrothermal loads, in their FE formulation for a symmetric finite width laminate under uniaxial tension. This formulation was based on the generalised plane strain approach. Wang and Dickinson (1976) applied the extended Galerkin method with displacements and interlaminar stresses satisfying the geometric boundary conditions represented by a complete set of Legendre polynomials. The final solutions were obtained by requiring the satisfaction of continuity conditions at

each interface and the stress boundary conditions at the exterior planes. Lee (1980) adopted three degrees-of-freedom per node for three-dimensional FE analysis of symmetric composite laminate with a center hole and subjected to biaxial inplane loads. Raju and Crews (1982) investigated edge stresses near the boundary of a circular hole in a symmetric cross-ply laminate using a quasi-three-dimensional FE analysis with 19000 degrees-of-freedom, i.e., a very fine mesh was used in the boundary layer region which provided more details in the neighbourhood of the singularity. They confirmed the presence of stress singularities and determined the power of singularity and the strength of singularity by assuming

$$\sigma = Ar^{-\lambda}$$

where A stands for the strength of singularity and λ, the power of singularity. They found these to be same for a number of ply combinations.

Pian (1973) developed the hybrid element and showed that because of the high accuracy of the hybrid elements, they are more efficient than the assumed displacement elements.

In the recent past, Spilker *et.al.* have developed stress formulation to analyse various types of plate problems based on different assumptions. Spilker and Chow (1980) analysed symmetric cross-ply laminates under uniform in-plane strain using the hybrid approach, in which, equilibrium in each layer, continuity of appropriate stresses and displacements at interface between layers and the traction free boundary conditions were satisfied exactly. They disscussed the importance of the satisfaction of the traction-free edge conditions. Non-satisfaction of these conditions could lead to a spurious or oscillating result in the boundary layer region. Spilker and Munir (1980) developed an assumed stress FE model for

the analysis of thin plates. They carried out a study for determining the criteria for the selection of stress assumptions to avoid element locking in the thin plate limit. They later (Spilker and Munir 1980) developed a hybrid stress element for the analysis of thin and moderately thick plates. They showed that the hybrid stress element yields better accuracy as compared to the assumed displacement based Mindlin plate element with reduced integration. Spilker (1980) developed a hybrid element for thick laminates wherein attention is restricted to the cylindrical bending. Spilker (1982) also developed a hybrid stress 8-node isoparametric multilayer plate element for the analysis of thin to thick fiber reinforced composite laminates.

Analytical solutions obtained by the use of complex potentials and eigen function series by Wang and Choi (1982) were used by Wang and Yuan (1983) to develop a singular hybrid element . This element, in conjunction with the conventional isoparametric quasi-three-dimensional elements has shown to be suitable for examining the detailed nature of boundary layer stresses in composite laminates.

1.3 Scope of Present Work :

The purpose of the present work is to analyse the edge effects in a symmetric , finite, multilayered rectangular composite laminate having a central circular/square hole. The present work uses the hybrid element developed by Spilker (1982) in conjunction with the singular element developed by Suresh (1987). The singular element is used in the boundary layer region while the hybrid element is used in the far field region. The exact order of singularity has been found by solving an eigen value

problem as done by Yamada (1983) and Suresh (1987). This has been used to construct singular hybrid elements while simpler hybrid stress variation is used for the far field elements.

The aim of the work is to ensure a computationally efficient method , by using a coarse mesh.

CHAPTER 2

PROBLEM DEFINITION

2.1 Introduction

In the present work, a composite plate with a hole has been analysed. The problem deals with the edge stresses in $[0/90]_S$ and $[90/0]_S$ laminate having a central circular/square hole. Due the complex nature of stresses a hybrid FEM approach has been employed. To simulate the edge singularities, a singular element approach has been used in the region close to the boundary.

2.2 Problem Definition

Figure2.1 shows a four ply laminate made of graphite/epoxy with each ply having thickness h. It has a central circular hole of radius r_o. Figure2.2 shows a similar laminate with a central square hole. These laminates are subjected to an uniform far-field displacement in the y-direction as shown. Each ply is idealised as homogenous, elastic, orthotropic material having following properties :

$E_{11} = 20 \times 10^6$ Psi (138 GPa)

$E_{22} = 2.1 \times 10^6$ Psi (14.5 GPa)

$G_{12} = 0.85 \times 10^6$ Psi (5.86 GPa)

$G_{23} = 0.85 \times 10^6$ Psi (5.86 GPa)

$\nu_{12} = 0.21$

$\nu_{23} = 0.21$

Here, the subscripts 1,2 and 3 refer to the material axes directions. Axis 1 is in the direction of the fibers and axis 2 is in the plane of the ply perpendicular to axis 1. Axis 3 is in the direction normal to the plane of the laminate.

The analysis has been carried out for two layup configurations viz. $[0/90]_s$ and $[90/0]_s$. Because of the symmetry in the problem, only one-eight of the laminate was analysed with the following boundary conditions :

i) Displacement boundary condition

a) $u = 0$ on $x = 0$

$v = 0$ on $y = 0$

$w = 0$ on $z = 0$

b) On the far end $y = 1$ plane

$u = u_0$ (constant)

ii) Traction boundary conditions :

a) Edges $x = b$, the top surface $z = 2h$, and the hole boundary $r = r0$ } Traction Free

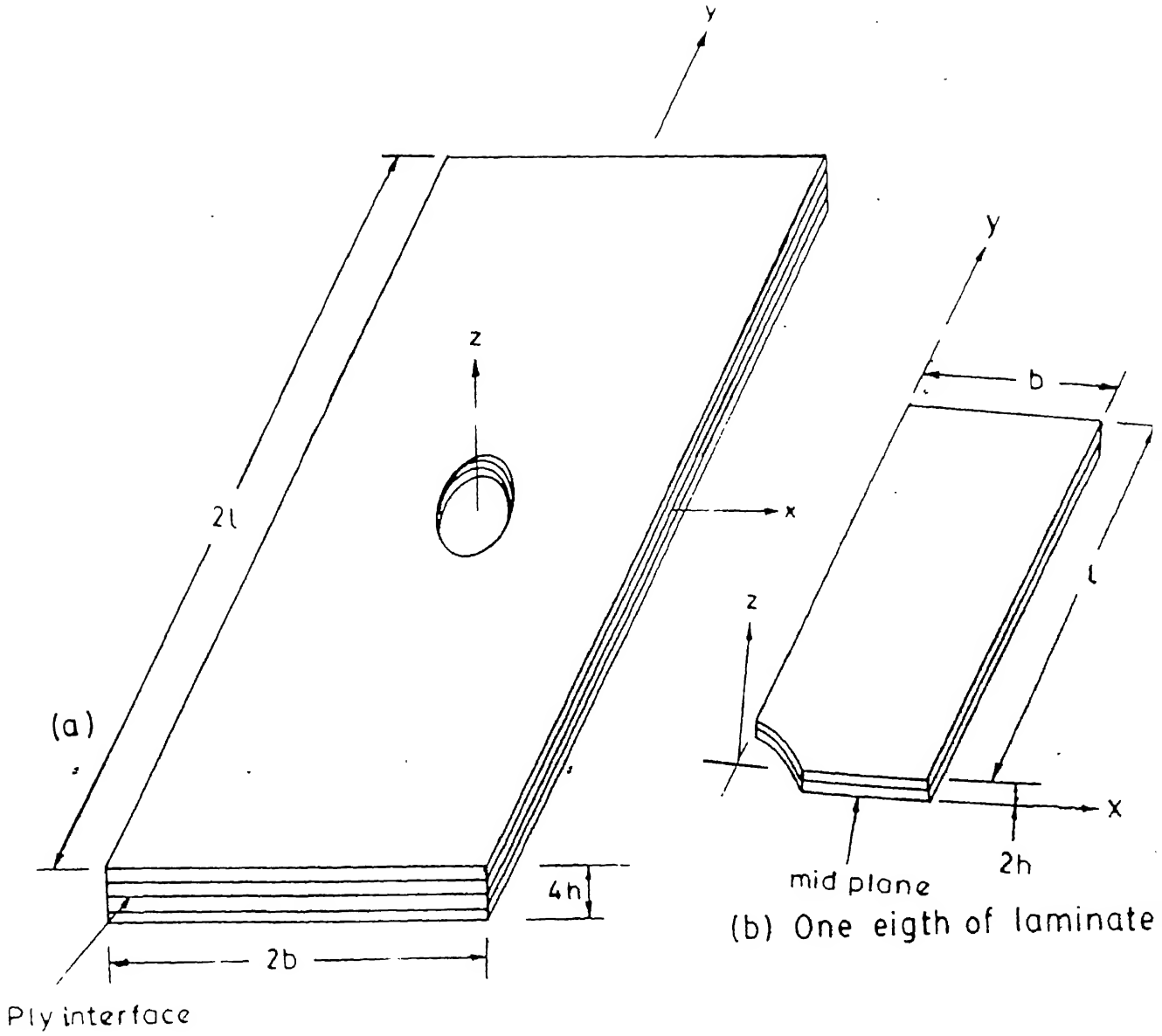

FIG. 2.1 GEOMETRY OF LAMINATE WITH A CIRCULAR HOLE

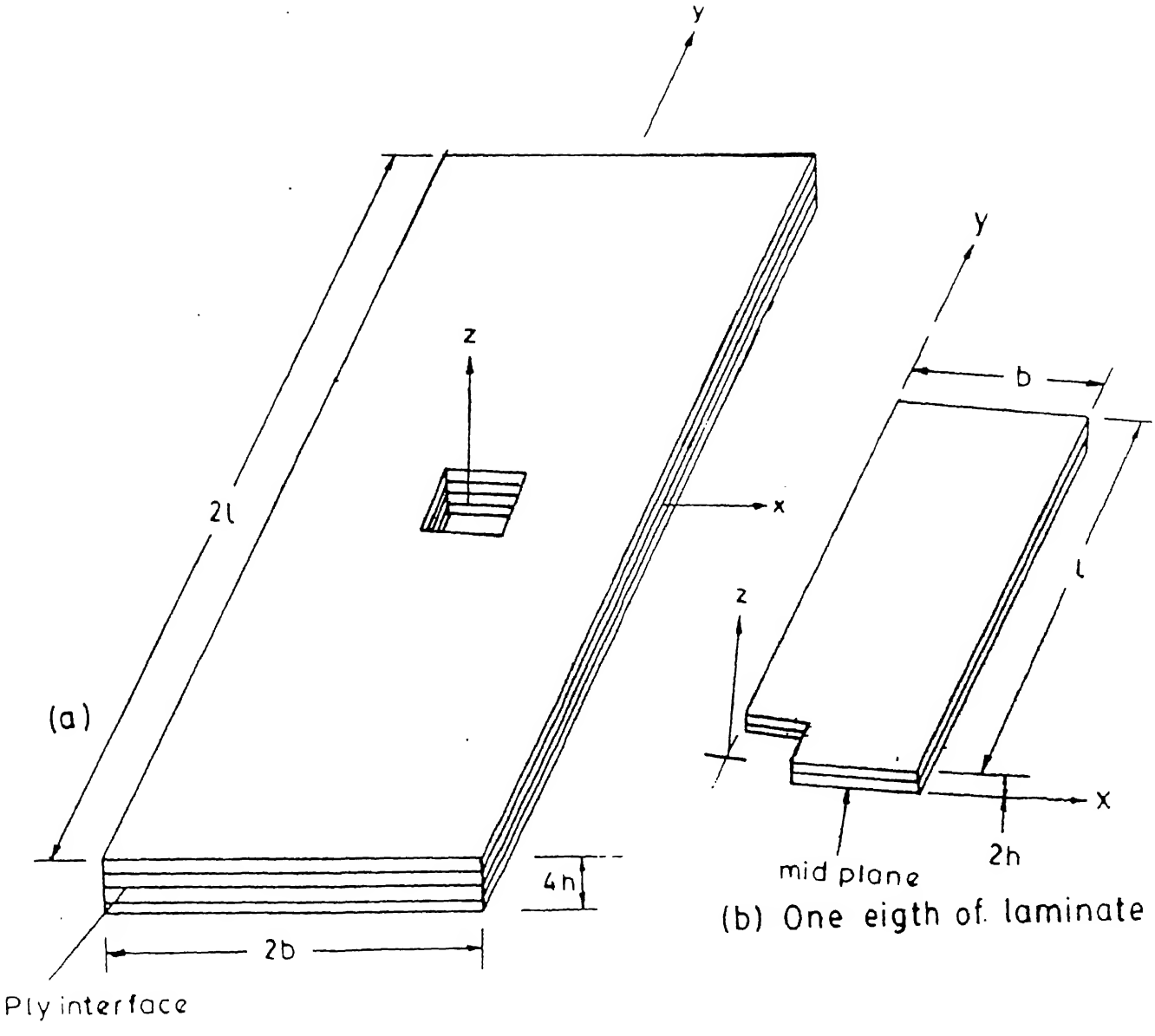

FIG. 2.2. GEOMETRY OF LAMINATE WITH A SQUARE HOLE

CHAPTER 3

THE SINGULAR HYBRID FEM APPROACH APPLIED TO LAMINATED PLATES

3.1 Introduction :

In problems of linear elasticity involving an interface joining two dissimilar materials, often complex states of stress are encountered. This is due to the existence of stress singularities in a localised region close to the free surface and at the interface. To obtain satisfactory results of such problems, as in the present case, a hybrid FEM approach in conjunction with the application of singular element in the boundary layer is the appropriate method.

In linear solid mechanics, the principle of minimum potential energy involves a compatible displacement field as its variable with the stress equilibrium equations and the traction boundary conditions as its Euler - Lagrange equations. The complimentary energy principle involves an equilibrated stress field satisfying the traction boundary conditions, as a variable with equations of kinematic compatability and displacement boundary conditions as its Euler - Lagrange equations.

For the solution of a linear boundary value problem by the finite element method by the application of the minimum potential energy principle, the displacement field should not only be continuous within the element but also be compatible at the interelement boundaries. The variational principle then gives (a) equilibrium within the element and (b) the traction reciprocity condition as the Euler-Lagrange equations. Similarly, for the application of complimentary energy principle, the stress field should satisfy the equilibrium equations and the interelement

traction reciprocity conditions. The Euler-Lagrange equations in this case are (a) the kinematic compatability within the element and (b) interelement displacement compatability.

For problems related to plate bending, shells, multilayered composites, problems with singularities, etc the application of the primal principles to FEM restrict the flexibility and do not give satisfactory solutions. To obtain this flexibility, one may relax the conditions of displacement continuity and/or traction reciprocity at the interelement boundaries on the admissible displacement/stress fields and introduce these as *posteriori* constraints by use of the Lagrange multiplier technique. This is the underlying concept of the Hybrid FEM methods.

If conventional displacement methods are used for the solution of problems involving stress singularities, a large number of elements have to be used to obtain credible results. On the contrary, the application of hybrid element formulations can ensure better results. However, even these methods do not guarantee convergence. This can be overcome by the use of appropriate singular element in conjunction with the hybrid FEM formulation, which will ensure efficiency in computation, and convergency of results.

3.2 Hybrid Stress Element :

These elements are refered to as the non-singular elements in the ensuing discussion. The elements considered here are assumed to lie in the x-y plane with the z-axis corresponding to the transverse direction. The element is composed of I perfectly bonded surfaces (interlayer surfaces and lower/upper surfaces) which are numbered from the bottom to top of

the laminate. The origin of the reference surface, z=0, is at the bottom and the location of each surface is given by $z=h_i$, ($h_1=0$), h_2, ..., h_{I+1} (see fig 3.1.). Each layer is of constant thickness and constant material properties (i.e. material constants in the material axis system, and ply/fiber orientation angle, θ), but thickness and properties may vary from layer to layer.

The elements used in the present problem are based on the hybrid stress model. The hybrid stress model uses a modified complimentary energy principle in which the interelement traction continuity and the mechanical boundary conditions have been relaxed via the Lagrange multilplier technique. The hybrid stress functional for multilayer element can be expressed as (Spliker 1982)

$$\pi_{mc} = \sum_{n}\sum_{I} \left\{ \frac{1}{2} \int_{V_{n_i}} \underline{\sigma}^{i^T} \underline{S}^i \underline{\sigma}^i \, dV - \int_{V_{n_i}} \underline{\sigma}^{i^T} \hat{\underline{\epsilon}}^i \, dV + \int_{S_{n_i}} \underline{u}^{i^T} \bar{\underline{T}}^i \, dS \right\} \quad (3.1)$$

where $\underline{\sigma}^i$ is the vector of stresses for layer i, $\hat{\underline{\epsilon}}^i$ is the vector of strains in the layer i computed (via strain-displacement relations) from displacements, $\underline{u}^i$, S^i is the Compliance matrix of the material ($\underline{\epsilon}^i = S^i \underline{\sigma}^i$, where $\underline{\epsilon}^i$ are actual strains, to be distinguished from $\hat{\underline{\epsilon}}^i$), $\bar{\underline{T}}^i$ are prescribed tractions, V_{n_i} is the volume of the layer i for element n, and $S_{\sigma_{n_i}}$ is the portion of the element boundary on which tractions are prescribed. The inner sum is over the layer I, while the outer sum is over the number of elements.

Each layer of the multilayer element is an unidirectional lamina and for the present purpose, is assumed to be homogenous and orthotropic . Material properties are specified with respect to the material axes (i.e.

co-ordinates X_1, X_2, X_3 where X_1 corresponds to the fiber direction, X_2 is the in-plane co-ordinate perpendicular to X_1, and X_3 is the transverse co-ordinate, refer fig. 3.2.). The required compliance matrix S^i relates stresses and strains in the global co-ordinate system (x,y,z). The material and global co-ordinates are related by the angle θ, where θ is the angle measured from the global axis x to the fiber direction X_i. Applying transformation laws and assuming stresses in the i^{th} layer as $\underline{\sigma}^{i^T} = [\, \sigma^i_x \;\; \sigma^i_y \;\; \sigma^i_z \;\; \sigma^i_{yz} \;\; \sigma^i_{xz} \;\; \sigma^i_{xy} \,]$, S^i is in the form

$$S^i = \begin{bmatrix} S_{11} & S_{12} & S_{13} & 0 & 0 & S_{16} \\ S_{12} & S_{22} & S_{23} & 0 & 0 & S_{26} \\ S_{31} & S_{32} & S_{33} & 0 & 0 & S_{36} \\ 0 & 0 & 0 & S_{44} & S_{45} & 0 \\ 0 & 0 & 0 & S_{54} & S_{55} & 0 \\ S_{61} & S_{62} & S_{63} & S_{64} & S_{65} & S_{66} \end{bmatrix}$$

where, with $m=\cos\theta$ and $n=\sin\theta$

$$S_{11} = \frac{m^4}{E_{11}} + \frac{n^4}{E_{22}} + m^2 n^2 \left(\frac{1}{G_{11}} - 2\frac{\nu_{12}}{E_{11}} \right)$$

$$S_{12} = m^2 n^2 \left(\frac{1}{E_{11}} + \frac{1}{E_{22}} - \frac{1}{G_{12}} \right) - (m^4 + n^4) \frac{\nu_{12}}{E_{11}}$$

$$S_{13} = -\left(m^2 \frac{\nu_{12}}{E_{11}} + n^2 \frac{\nu_{12}}{E_{22}} \right)$$

$$S_{16} = 2mn \left(\frac{m^2}{E_{11}} - \frac{n^2}{E_{22}} \right) - mn\,(m^2 - n^2) \left(\frac{1}{G_{12}} - \frac{\nu_{12}}{E_{11}} \right)$$

$$S_{22} = \frac{n^4}{E_{11}} + \frac{m^4}{E_{22}} + m^2 n^2 \left(\frac{1}{G_{12}} - 2\frac{\nu_{12}}{E_{11}} \right)$$

$$S_{23} = -\left(n^2 \frac{\nu_{12}}{E_{11}} + m^2 \frac{\nu_{12}}{E_{22}} \right)$$

$$S_{26} = 2mn \left(\frac{n^2}{E_{11}} - \frac{m^2}{E_{22}} \right) - mn\,(m^2 - n^2) \left(\frac{1}{G_{12}} - \frac{\nu_{12}}{E_{11}} \right)$$

$$S_{33} = \frac{1}{E_{22}}$$

$$S_{36} = mn \left(\frac{\nu_{23}}{E_{22}} + \frac{\nu_{12}}{E_{11}} \right)$$

$$S_{44} = \frac{m^2}{G_{23}} + \frac{n^2}{G_{12}}$$

$$S_{45} = mn \left(\frac{1}{G_{12}} - \frac{1}{G_{23}} \right)$$

$$S_{55} = \frac{n^2}{G_{23}} + \frac{m^2}{G_{12}}$$

$$S_{66} = 4m^2 n^2 \left(\frac{1}{E_{11}} + \frac{1}{E_{22}} + \frac{\nu_{12}}{G_{12}} \right) - (m^2 - n^2) \frac{1}{G_{12}} \qquad (3.2)$$

In equation (3.2), E_{11} and E_{22} are Young's moduli in the fiber and transverse directions respectively, ν_{12} and ν_{23} are the major and minor Poisson's ratios.

Returning now to the element formulation based on equation (3.1),

stresses in the layer are assumed in terms of a finite set of stress parameters, $\underline{\beta}^i$, for layer i, in the form

$$\underline{\sigma}^i = P^i \, \underline{\beta}^i \tag{3.3}$$

where P^i consists of polynomial terms and is defined so that the homogeneous equilibrium equations are exactly satisfied. The typical set of polynomials used for the present analysis are given in Appendix-A.

The isoparametric transformation used in the present 8-noded element is

$$x = \sum_{j=1}^{8} N_j \, (\xi,\eta) \, x_j \tag{3.4}$$

$$y = \sum_{j=1}^{8} N_j \, (\xi,\eta) \, y_j \tag{3.5}$$

where $N_j \, (\xi,\eta)$ corresponds to the biquadratic serendipity shape functions (given in the Appendix-B) and (x_j,y_j) are the global in-plane co-ordinates of the node j. In addition, a normalised transverse co-ordinate, τ, is introduced for each layer which is related to z by

$$z = \tfrac{1}{2} \, [(h_i + h_{i+1}) + \tau \, (h_{i+1} + h_i)] \tag{3.6}$$

so that τ takes the value -1 at the bottom of the layer i and +1 at the top of the layer i. Using Eqs. (3.4 - 3.6), P^i in the x,y,z co-ordinates can be expressed in terms of normalised co-ordinates (ξ,η,τ).

The displacements $\underline{u}^i$ for the layer i are interpolated in terms of nodal displacements, $\underline{q}^i$, for layer i in the form of

$$\underline{u}^i = N^i \, \underline{q}^i \tag{3.7}$$

where N^i are the shape functions in the normalised co-ordinates (ξ,η,τ). Here, $\underline{u}^i$ is to be ordered as $\underline{u}^{i\,T} = [\, u \; v \; w \,]^i$ (displacements in the x,y and z

directions respectively). By applying the linear strain-displacement relations to Eq. (3.7), the strains $\hat{\underline{\varepsilon}}^i$ can be related to $\underline{q}^i$ as

$$\hat{\underline{\varepsilon}}^i = D^i \underline{u}^i = D^i N^i \underline{q}^i = B^i \underline{q}^i = \frac{1}{|J|} B^{*i} \underline{q}^i \qquad (3.8)$$

where D^i is the strain-displacement differential operator matrix, and $|J|$ is the Jacobian of the transformation given by the Eq (3.4 - 3.5). If the components of $\hat{\underline{\varepsilon}}^i$ are ordered as in $\underline{\sigma}^i$, D^i is given by

$$D^i = \frac{1}{|J|} \begin{bmatrix} \left(\frac{\partial y}{\partial \eta}\frac{\partial}{\partial \xi} - \frac{\partial y}{\partial \xi}\frac{\partial}{\partial \eta}\right) & 0 & 0 \\ 0 & \left(\frac{\partial y}{\partial \xi}\frac{\partial}{\partial \eta} - \frac{\partial x}{\partial \eta}\frac{\partial}{\partial \xi}\right) & 0 \\ 0 & 0 & \frac{|J|}{\bar{t}_i}\frac{\partial}{\partial \xi} \\ 0 & \frac{|J|}{\bar{t}_i}\frac{\partial}{\partial \xi} & \left(\frac{\partial x}{\partial \xi}\frac{\partial}{\partial \eta} - \frac{\partial x}{\partial \eta}\frac{\partial}{\partial \xi}\right) \\ \frac{|J|}{\bar{t}_i}\frac{\partial}{\partial \xi} & 0 & \left(\frac{\partial y}{\partial \eta}\frac{\partial}{\partial \xi} - \frac{\partial y}{\partial \xi}\frac{\partial}{\partial \eta}\right) \\ \left(\frac{\partial x}{\partial \xi}\frac{\partial}{\partial \eta} - \frac{\partial x}{\partial \eta}\frac{\partial}{\partial \xi}\right) & \left(\frac{\partial y}{\partial \eta}\frac{\partial}{\partial \xi} - \frac{\partial y}{\partial \xi}\frac{\partial}{\partial \eta}\right) & 0 \end{bmatrix} \qquad (3.9)$$

where the transformation of Eq. (3.4 - 3.5) is used in Eq. (3.9) and $\bar{t}_i$ is half the thickness of layer i, i.e.

$$\bar{t}_i = \left(\frac{h_{i+1} - h_i}{2}\right) \qquad (3.10)$$

Substituting eqs. (3.3), (3.7), and (3.8) into Eq (3.1) and using the following layer matrices :

$$H^i = \bar{t}_i \int_{-1}^{1}\int_{-1}^{1}\int_{-1}^{1} P^{i\,T} S^i P^i \; |J| \; d\xi \, d\eta \, d\tau \qquad (3.11)$$

$$G^i = \bar{t}_i \int_{-1}^{1} \int_{-1}^{1} \int_{-1}^{1} P^{i^T} B^{*i} \, d\xi \, d\eta \, d\tau \tag{3.12}$$

$$Q^i = \int_{S\sigma_{n_i}} N^{i^T} \bar{T}^i \, ds \tag{3.13}$$

π_{mc} becomes

$$\pi_{mc} = \sum_n \sum_I \left\{ \tfrac{1}{2} \underline{\beta}^{i^T} H^i \underline{\beta}^i - \underline{\beta}^{i^T} G^i \underline{q}^i + \underline{q}^{i^T} Q^i \right\} \tag{3.14}$$

At this stage, stresses and displacements are independant from layer to layer. However, enforcement of traction continuity along interlayer surfaces will require that certain of the β^{i+1} be related to certain of the β^i (i.e. at the interface between layers i and i+1). Similarly certain of the nodal displacements, q^{i+1}, will be related to certain q^i in order to satisfy displacement continuity along the interlayer surface between layers i and i+1.

Corresponding to these interlayer surface continiuity conditions, layer stress parameters, β^i, and nodal displacements, q^i, can be related to the overall laminate stress parameters, $\underline{\beta}$, and nodal displacements $\underline{q}$, respectively, in the form :

$$\underline{\beta}^i = C_s{}^i \, \underline{\beta} \tag{3.15}$$

$$\underline{q}^i = C_d{}^i \, \underline{q} \tag{3.16}$$

By substituting above equations into Eq.(3.14), π_{mc} is now simplified in terms of laminate/element stress and displacement parameters and from Eq.(3.1), is given by

$$\pi_{mc} = \sum_n \left\{ \tfrac{1}{2} \underline{\beta}^T H \underline{\beta} - \underline{\beta}^T G \underline{q} + \underline{q}^T Q \right\} \tag{3.17}$$

where

$$H = \sum_{I} {C_s}^{i^T} H^i {C_s}^i \tag{3.18}$$

$$G = \sum_{I} {C_s}^{i^T} G^i {C_d}^i \tag{3.19}$$

$$Q = \sum_{I} {C_d}^{i^T} Q^i \tag{3.20}$$

In the above equations matrix multiplications are not carried out explicitly. The operations in the above equations are simmilar to element assembly operations; a set of layer to laminate parameter 'pointers' and nodal displacement 'pointers' can be used to locate layer matrix contributions in the laminate matrices.

The variation of functional π_{mc} with respect to β yeilds the set of equations

$$H\underline{\beta} - G\underline{q} = 0 \tag{3.21}$$

Hence,

$$\underline{\beta} = H^{-1} G \underline{q} \tag{3.22}$$

and taking variation with respect to $\underline{q}$

$$G^T \underline{\beta} = Q \tag{3.23}$$

Substituting eq.(3.22) into eq.(3.23)

$$G^T H^{-1} G \underline{q} = Q \tag{3.24}$$

Rewriting the equation in the form

$$k \underline{q} = Q$$

The elemental stiffness matrix can be identified as

$$K = G^T H^{-1} G \tag{3.25}$$

and Q as the elemental load vector.

Once the nodal displacements have been calculated, stresses for each layer are calculated by obtaining $\underline{\beta}$ from Eq. (3.22), $\underline{\beta}^i$ from Eq. (3.15) (by extracting the appropriate $\underline{\beta}^i$ from $\underline{\beta}$), and substituting into Eq. (3.3). Strains $\underline{\varepsilon}^i$ can be obtained from stresses $\underline{\sigma}^i$ by using S^i.

3.2.1 Displacement Interpolation for a Layer :

Moderately thin and thick laminates are characterised by severe crosssectional warping, and each layer must be allowed to undergo non-normal crosssection rotations, while preserving interlayer surface displacement continuity. To incorporate this warping behaviour, all displacement components (u,v and w in x, y and z directions, respectively) are assumed to vary linearly, through the thickness of each layer. The degrees of freedom at any node j, which guarantees interlayer surface displacement continuity, are therefore u^i_j, v^i_j and w^i_j where, i signifies the points at the bottom, each interlayer and upper surface for this node (i = 1,2,3 ....., I+1) (Fig 3.3). The displacement interpolations in normalised coordinates for typical layer i are then given as

$$u^i(\xi,\eta,\tau) = \sum_{j=1}^{8} N_j(\xi,\eta)\left[\tfrac{1}{2}(1-\tau)\,u_j^i + \tfrac{1}{2}(1+\tau)\,u_j^{i+1}\right] \tag{3.26}$$

$$v^i(\xi,\eta,\tau) = \sum_{j=1}^{8} N_j(\xi,\eta)\left[\tfrac{1}{2}(1-\tau)\,v_j^i + \tfrac{1}{2}(1+\tau)\,v_j^{i+1}\right] \tag{3.27}$$

$$w^i(\xi,\eta,\tau) = \sum_{j=1}^{8} N_j(\xi,\eta)\left[\tfrac{1}{2}(1-\tau)\,w_j^i + \tfrac{1}{2}(1+\tau)\,w_j^{i+1}\right] \tag{3.28}$$

where N_j (ξ,η) are the standard 8-node biquadratic Serendipity shape functions (shown in Appendix-B).

The u_j^i, u_j^{i+1}, v_j^i, v_j^{i+1}, w_j^i, w_j^{i+1}, are treated as the layer degrees-of-freedom, $\underline{q}^i$; Eqs. (3.26 - 3.28) then define N^i of Eq. (3.7), from which B^{*i} of Eq. (3.8) can be computed. The ordering of laminate degrees of freedom is given by,

$$q^T=[u_1^1 u_1^2 \ldots u_1^{I+1} v_1^1 v_1^2 \ldots v_1^{I+1} w_1^1 w_1^2 \ldots w_1^{I+1}\ u_2^1 u_2^2 \ldots u_2^{I+1}\ v_2^1 v_2^2 \ldots v_2^{I+1}$$
$$w_2^1 w_2^2 \ldots w_2^{I+1} \ldots\ldots\ldots u_8^1 u_8^2 \ldots u_8^{I+1} v_8^1 v_8^2 \ldots v_8^{I+1} w_8^1 w_8^2 \ldots w_8^{I+1}] \quad (3.29)$$

the Boolean matrix C_d^i of Eq. (3.16) can be defined. For I layers, the 8-node element based on the 'general' displacement field of Eqs. (3.26 - 3.28) will have 24(I+1) total degrees of freedom per element and 3(I+1) degrees of freedom per node.

3.3 Layer Stress Interpolation for Non-singular Hybrid and Singular Hybrid Elements :

In the present formulation, two types of elements are used. Adjacent to the hole boundary, the stresses are singular and hence singular hybrid elements are employed. In the region away from the hole boundary, the non-singular hybrid elements have been used.

3.3.1 Stress Interpolation for Non-singular Elements :

All components of stresses are included and are interpolated within each layer in terms of stress parameters, $\underline{\beta}^i$, for that layer, such that

homogenous equilibrium equations are exactly satisfied. Introducing the normalised transverse layer co-ordinate, τ, these equations are

$$\frac{\partial \sigma_x^i}{\partial x} + \frac{\partial \sigma_{xy}^i}{\partial y} + \frac{1}{t_i}\frac{\partial \sigma_{xz}^i}{\partial \tau} = 0 \qquad (3.30)$$

$$\frac{\partial \sigma_{xy}^i}{\partial x} + \frac{\partial \sigma_y^i}{\partial y} + \frac{1}{t_i}\frac{\partial \sigma_{yz}^i}{\partial \tau} = 0 \qquad (3.31)$$

$$\frac{\partial \sigma_{xz}^i}{\partial x} + \frac{\partial \sigma_{yz}^i}{\partial y} + \frac{1}{t_i}\frac{\partial \sigma_z^i}{\partial \tau} = 0 \qquad (3.32)$$

The stresses $\sigma_x^i(x,y,\tau)$, $\sigma_y^i(x,y,\tau)$, $\sigma_z^i(x,y,\tau)$ are assumed to vary linearly in τ within the layer. Then from Eqs. (3.30) and (3.31), $\sigma_{xz}^i(x,y,\tau)$ and $\sigma_{yz}^i(x,y,\tau)$ must be of the order τ^2, from Eq. (20.3) $\sigma_z^i(x,y,\tau)$ must be of the order τ^3 within the layer. A 67 term (67 β's), generalised hybrid stress assumption used in the present analysis is presented in Appendix-A. It may be noted that the stretching portions of σ_x^i, σ_y^i, σ_{xy}^i, remain complete cubic polynomials in x, y, σ_{xz}^i and σ_{yz}^i include all quadratic x, y terms and σ_z^i is linear in x and y.

The layer stress fields satisfy the homogenous equilibrium equations within the layer, but stress parameters are independant from layer to layer. In the the present element used, the interlayer traction continuity are satisfied by establishing a set of element/laminate stress parameters, β, and relating $\underline{\beta}^i$ to $\underline{\beta}$ as in Eq. (3.15).

The interlayer surface traction continuity requires that σ_{xz}, σ_{yz} and σ_z be continuous at interlayer surfaces. For example for the polynomials assumed in the present analysis (Appendix-A), evaluation of these stresses at the lower surface (τ = -1) of layer i yields :

$$\sigma^i_{xz}|_{\tau=-1} = \bar{t}_i \left(\beta_1{}^i + \beta_2{}^i x + \beta_3{}^i y + \beta_4{}^i x^2 + \beta_5{}^i xy + \beta_6{}^i y^2 \right)$$

$$\sigma^i_{yz}|_{\tau=-1} = \bar{t}_i \left(\beta_7{}^i + \beta_8{}^i x + \beta_9{}^i y + \beta_{10}{}^i x^2 + \beta_{11}{}^i xy + \beta_{12}{}^i y^2 \right) \qquad (3.32)$$

$$\sigma^i_{z}|_{\tau=-1} = \bar{t}^2_i \left(\beta_{13}{}^i + \beta_{14}{}^i x + \beta_{15}{}^i y \right)$$

and the upper surface ($\tau = 1$) of layer i :

$$\sigma^i_{xz}|_{\tau=+1} = \bar{t}_i \left(\beta_{53}{}^i + \beta_{54}{}^i x + \beta_{55}{}^i y + \beta_{56}{}^i x^2 + \beta_{57}{}^i xy + \beta_{58}{}^i y^2 \right)$$

$$\sigma^i_{yz}|_{\tau=+1} = \bar{t}_i \left(\beta_{59}{}^i + \beta_{60}{}^i x + \beta_{61}{}^i y + \beta_{62}{}^i x^2 + \beta_{63}{}^i xy + \beta_{64}{}^i y^2 \right) \qquad (3.33)$$

$$\sigma^i_{z}|_{\tau=+1} = \bar{t}^2_i \left(\beta_{65}{}^i + \beta_{66}{}^i x + \beta_{67}{}^i y \right)$$

With the simple form of transverse shear and normal stresses at interlayer surfaces, the traction continuity condition at the interface between layers i-1 and i (where i > 1) requires that

$$\beta_j{}^i = \frac{\bar{t}_{i-1}}{\bar{t}_i} \beta_{j+52}{}^{i-1} \qquad j = 1,2,\ldots,12 \qquad (3.34)$$

$$\beta_j{}^i = \frac{\bar{t}^2_{i-1}}{\bar{t}^2_i} \beta_{j+52}{}^{i-1} \qquad j = 13,14,15 \qquad (3.35)$$

thus the set of independant laminate stress parameters, β, for the present element is reduced to

$$\underline{\beta}^T = [\ \beta^1_1 \beta^1_2 \ldots\ldots \beta^1_{67}\ \beta^2_{16} \beta^2_{17} \ldots\ldots \beta^2_{67}\ \beta^I_{16} \beta^I_{17} \ldots\ldots \beta^I_{67}\ ] \qquad (3.36)$$

Thus the total number of independant stress parameters for I layer laminate is (67 - 15) I.

The $C_S{}^i$ of Eq (3.15) can be constructed for each layer using Eqs. (3.34 - 3.35) and the laminate $\underline{\beta}$ of Eq (3.36). In practice, matrix multiplications in Eq. (3.17) and (3.18) involving $C_S{}^i$ are not performed. Instead, row and column H^i and rows in G^i corresponding to β^i_1 - β^i_{15} are scaled as per Eqs. (3.34 - 3.35), after which a set of layer-to-laminate stress parameter 'pointers' are used to appropriately assemble the scaled H^i into H and G into G^i.

3.3.2 Stress Interpolation for the Singular Element :

In the present problem of analysing crossply composite laminates with a central hole, subjected to far-field loads, the stresses near the boundary will be very large and three-dimensional in nature (theoretically, some of the components are singular). As the singularity is due to the interaction of the free edge (circular hole boundary) and the material discontinuity between layers, it can be observed that the severity of the stress singularity changes from point to point along the hole boundary. Such a problem is truely three-dimensional in nature and no work has been reported so far to solve this problem. However, work was reported (Yamada(1983) and Suresh(1987)) wherein, the severity or the power of singularuity was determined for an axisymmetric cases.

To determine the singularity as a first step and its use in the hybrid formulation, a simplified procedure along with a few assumptions is adopted.

- At each poimt along the hole boundary, the radial and tangential (r,θ) material properties are determined and the singularity index at that point is found under the assumption that the same conditions prevail all along the boundary - thus leading to the axisymmetric nature. As can be observed, the following two factors are neglected viz.

1. The variation of the material properties along the tangential direction near the hole boundary, and

2. The non-axisymmetric nature of the farfield loads.

The effect of these two factors in the stress singularity may be assumed to be marginal because of the fact that stress singularities arise mainly due to the free edges (intersection of the hole boundary and the material discontinuity in the thickness direction) and the axisymmetric assumption is used in regions close to the hole boundary. Also, the power of singularity can be very easily determined for an axisymmetric case. This stress approximation is then required to satisfy

$$\frac{\partial \sigma_r}{\partial r} + \frac{\partial \tau_{rz}}{\partial z} + \frac{\sigma_\theta - \sigma_r}{r} = 0 \tag{3.37}$$

$$\frac{\partial \tau_{rz}}{\partial r} + \frac{\partial \sigma_z}{\partial z} + \frac{\tau_{rz}}{r} = 0 \tag{3.38}$$

As the interlaminar stresses σ_z, τ_{rz} and the in-plane stress σ_θ show singularities, the following approximations have been used for these stresses and the other stress components are then found by enforcing the stress equilibrium conditions.

$$\sigma_z = \beta_i \left((r - r_o)^2 + z^2 \right)^{\lambda} \tag{3.39}$$

$$\tau_{rz} = \beta_j \left((r - r_o)^2 + z^2 \right)^{\lambda} \tag{3.40}$$

$$\sigma_\theta = \beta_k \left((r - r_o)^2 + z^2 \right)^{\lambda} \tag{3.41}$$

The contributions from these stress terms are introduced into the

layer stress interpolation discussed in the previous section as follows: These terms are added to the 67 polynomial approximation to make it a 70 term polynomial. To facilitate the programming of this condiotion, the β's from the top layer are introduced as β_{16} - β_{18} shifting the β's from the bottom layer to β_{71} - β_{73}. Hence, in Eqs. (3.39 - 3.41),

i = 71, j = 72 and k = 73 for the bottom layer

while i = 16, j = 17 and k = 18 for the top layer

r_o = hole radius

λ = power of singularity

Substituting Eq. (3.39) in equation Eq. (3.38),

$$\tau_{rz} = - \frac{1}{r} \beta_i \lambda z \int_{r_o}^{r} r \left((r - r_o) + z^2 \right)^{\frac{\lambda}{2} - 1} dr \qquad (3.42)$$

Solving this integral, the solution in terms of the Gauss Hypergeometric series is as follows

$$\tau_{rz} = - \frac{1}{r} \beta_i \lambda z \left(\frac{1}{\lambda} \left((s^2 + z^2)^{\frac{\lambda}{2}} - z^{\lambda} \right) + r0\, z^{\lambda - 1} \left(\left(\frac{s^2}{s^2 + z^2} \right)^{\frac{1}{2}} \right.\right.$$

$$\left.\left. + \frac{\alpha \beta}{\gamma} \left(\frac{s^2}{s^2 + z^2} \right)^{\frac{3}{2}} + \frac{\alpha \beta}{\gamma} \frac{(\alpha + 1)(\beta + 1)}{(\gamma + 1)\, 2\, !} \left(\frac{s^2}{s^2 + z^2} \right)^{\frac{5}{2}} + \ldots \right) \right) \qquad (3.43)$$

As this series converges quickly, only the first three terms of the series have been considered for the present formulation.

At the hole boundary,

$\sigma_r = 0$, as the boundary condition. (3.44)

Substituting Eq. (3.43) and Eq. (3.44) in Eq.(3.37),

$$\sigma_\theta = -\beta_j \left(\lambda z^2 (s^2 + z^2)^{\frac{\lambda}{2}} - 1 + (s^2 + z^2)^{\frac{\lambda}{2}} - (\lambda + 1) z^\lambda + r_o \lambda \left(-z^{\lambda+1} \right.\right.$$

$$\left(s(s^2 + z^2)^{-\frac{3}{2}} + \frac{3\,\alpha\beta}{\gamma} s^3 \left(s^2 + z^2 \right)^{-\frac{5}{2}} + \frac{5\,\alpha\beta}{\gamma} \frac{(\alpha + 1)(\beta + 1)}{(\gamma + 1)} s^5 (s^2 + z^2)^{-\frac{7}{2}} \right.$$

$$\left. + \ldots\ldots \right) + \lambda z^{\lambda - 1} \left(\left(\frac{s^2}{s^2 + z^2} \right)^{\frac{1}{2}} + \frac{\alpha\,\beta}{\gamma} \left(\frac{s^2}{s^2 + z^2} \right)^{\frac{3}{2}} + \frac{\alpha\beta}{\gamma} \frac{(\alpha + 1)(\beta + 1)}{(\gamma + 1)\,2\,!} \right.$$

$$\left. \left. \left(\frac{s^2}{s^2 + z^2} \right)^{\frac{5}{2}} + \ldots\ldots \right) \right) \right) \qquad (3.45)$$

Here,

$$s = r - r_o$$

$$\alpha = \tfrac{1}{2}$$

$$\beta = \tfrac{1+\lambda}{2}$$

$$\gamma = \tfrac{3}{2}$$

Substituting τ_{rz} from Eq.(3.40) into Eq.(3.38)

$$\sigma_z = -\tfrac{1}{r}\,\beta_j\, s^{(\lambda+1)} \left(\frac{s^2}{s^2 + z^2} \right)^{\frac{1}{2}} {}_2F_1' - \beta_j \lambda\, s^\lambda \left(\frac{s^2}{s^2 + z^2} \right)^{\frac{1}{2}} {}_2F_1 \qquad (3.46)$$

where , ${}_2F_1$ is the hypergeometric series

For ${}_2F_1'$, $\alpha = \frac{1}{2}$, $\beta = \frac{3+\lambda}{2}$ and $\gamma = \frac{3}{2}$

From Eq.(3.37)

$$\sigma_\theta = r^{\frac{\lambda}{2}} z\ \beta_j \left((r - r_o)^2 + z^2 \right)^\lambda \qquad (3.47)$$

Finally, substituting Eq.(3.41) into Eq.(3.37)

$$\tau_{rz} = \beta_k \frac{1}{r} s^{(\lambda+1)} \left(\frac{s^2}{s^2 + z^2} \right)^{\frac{1}{2}} {}_2F_1 \tag{3.48}$$

From Eq.(3.38)

$$\sigma_z = - \frac{1}{r} \beta_k (\lambda+1) s^{\lambda} \left((s^2+z^2)^{\frac{1}{2}} + \frac{\alpha\beta}{\gamma} \left(\frac{s^2}{(s^2+z^2)^{\frac{1}{2}}} + (s^2+z^2)^{\frac{1}{2}} \right) \right.$$

$$\left. + \frac{1}{2!} \frac{\alpha\beta}{\gamma} \frac{(\alpha+1)(\beta+1)}{(\gamma+1)} \left((s^2+z^2)2 + \frac{2s^2}{(s^2+z^2)^{\frac{1}{2}}} - \frac{1}{3} \frac{s^4}{(s^2+z^2)^{\frac{3}{2}}} \right) \right)$$

$$- \frac{1}{r} \beta_k s^{(\lambda+2)} \left(\left(\frac{1}{(s^2+z^2)^{\frac{1}{2}}} + \frac{\alpha\beta}{\gamma} \left(\frac{1}{(s^2+z^2)^{\frac{1}{2}}} - \frac{1}{3} \frac{s^2}{(s^2+z^2)^{\frac{3}{2}}} \right) \right) \right.$$

$$\left. + \frac{1}{2!} \frac{\alpha\beta}{\gamma} \frac{(\alpha+1)(\beta+1)}{(\gamma+1)} \left(\frac{1}{(s^2+z^2)^{\frac{1}{2}}} - \frac{2s^2}{3(s^2+z^2)^{\frac{3}{2}}} - \frac{1}{5} \frac{s^4}{(s^2+z^2)^{\frac{5}{2}}} \right) \right) \tag{3.49}$$

These stress components which are in cylindrical co-ordinates, are transformed to the Cartesian system using the transformation matrix.

The contribution from these singular terms is then introduced as the coefficients of β_{71} - β_{73} for layer i and the coefficient of β_{16} - β_{18} for the layer i+1. The assembly procedure and the calculation of the H, G and the stiffness matrix K remains the same as has been discussed previously.

3.3.3 Determination of the Power of Singularity

A finite element analysis has been carried out to determine the power of singularity (Yamada 1983 and Suresh 1987). For the axisymmetric case, the singular elements are a triangular sector spread across the hole

boundary as shown in the fig 3.4. In this approach, the singularity is determined by the use of isoparametric mapping. For the sake of completeness, this approach is explained in this section. The mapping is as follows.(fig.3.5)

$$s = \left(\frac{1+\xi}{2}\right) s_0 \tag{3.50}$$

$$\rho = \frac{r}{r_0} = \left(\frac{1+\xi}{2}\right)^{\frac{1}{\lambda}} \tag{3.51}$$

and

$$\theta = H_1\,\theta_1 + H_2\,\theta_2 + H_3\,\theta_3 \tag{3.52}$$

where

$$H_1 = \tfrac{1}{2}\left(-\eta + \eta^2\right),\quad H_2 = 1 - \eta^2,\quad H_3 = \tfrac{1}{2}\left(\eta + \eta^2\right) \tag{3.53}$$

are the shape functions and, s and θ represent the polar coordinate radius and the angle of a generic point P, s_0 being the radius of the common circular arc on which the nodes 1, 2 and 3 are placed.

A consistent isoparametric displacement field has been used as follows

$$u - u_s = \left[\, H_1\,(u_1 - u_s) + H_2\,(u_2 - u_s) + H_3\,(u_3 - u_s)\,\right]\left(\frac{1+\xi}{2}\right) \tag{3.54}$$

where u_s represents the displacement vector at the vertex S of the sector and u_i(i=1, 2, 3) are the displacement vectors at the nodes on the circular arc of radius $s = s_0$. Substituting Eq. (3.51) in Eq. (3.54) gives rise to a term ρ^{λ} in the expression for the displacement field. Hence, the singularity of stress and strain thus introduced is in the order of $\rho^{\lambda-1}$.

The next step is to formulate the pertinent eigen value problem, which is done by solving the following axisymmetric finite element problem.

The co-ordinates r and z, or the position of any point on the sector on the axisymmetric plane is given by

$$r = a + s\cos\theta \tag{3.55}$$

$$z = s\sin\theta \tag{3.56}$$

as shown in the fig 3.5.

The displacement vector is given by

$$u = \begin{Bmatrix} u_r \\ u_z \end{Bmatrix} \tag{3.57}$$

Expressing strains in terms of displacements, for the axisymmetric case

$$\begin{matrix} \epsilon_r \\ \epsilon_z \\ \epsilon_\theta \\ \gamma_{rz} \end{matrix} = \begin{Bmatrix} \dfrac{\partial \bar{u}_r}{\partial r} \\ \dfrac{\partial \bar{v}_z}{\partial z} \\ \dfrac{\bar{u}_r}{r} \\ \dfrac{\partial \bar{u}_r}{\partial r} + \dfrac{\partial \bar{v}_z}{\partial z} \end{Bmatrix} \tag{3.58}$$

The detailed derivation for the expressions for ϵ_r, ϵ_z, ϵ_θ and γ_{rz} are as given in reference Suresh(1987) which are obtained from Eqs. (3.50 - 3.57). This leads to

$$\{ \epsilon \} = [B] \{u_i\} \tag{3.59}$$

where $$[B] = \frac{\rho^{\lambda-1}}{s_0} [\lambda [B_a] + [B_b]] \tag{3.60}$$

From the virtual work principle for the domain, the following expression can be had,

$$\int_{-1}^{1} \int_{-1}^{1} (\sigma_r \, \partial\epsilon_r + \sigma_z \, \partial\epsilon_z + \sigma_\theta \, \partial\epsilon_\theta + \tau_{rz} \, \partial\gamma_{rz}) \, 2\pi \, r_{cg} \, dr \, dz$$

$$= \int_{-1}^{1} (T_r \, \partial\bar{u}_r + T_z \, \partial\bar{v}_z + T_{rz} \, \partial\bar{u}_r \, \partial\bar{v}_z) \, 2\pi \, r_{cn} \, d\theta \qquad (3.61)$$

where r_{cg} is the radius of the centroid of the element and r_{cn} is the radius of the node on the circular boundary with respect to the hole center.

Substituting Eq.(3.60) into Eq.(3.61), the characteristic equation in λ is of the form

$$\lambda^2 [A] + \lambda [B] + [C] = 0 \qquad (3.62)$$

which is then reduced to an eigen value problem for solution of λ. The matrices [A], [B] and [C] are given in reference Suresh(1987).

This eigen value problem has been solved for points along the hole boundary in order to determine the order of singularity as an angular variation.

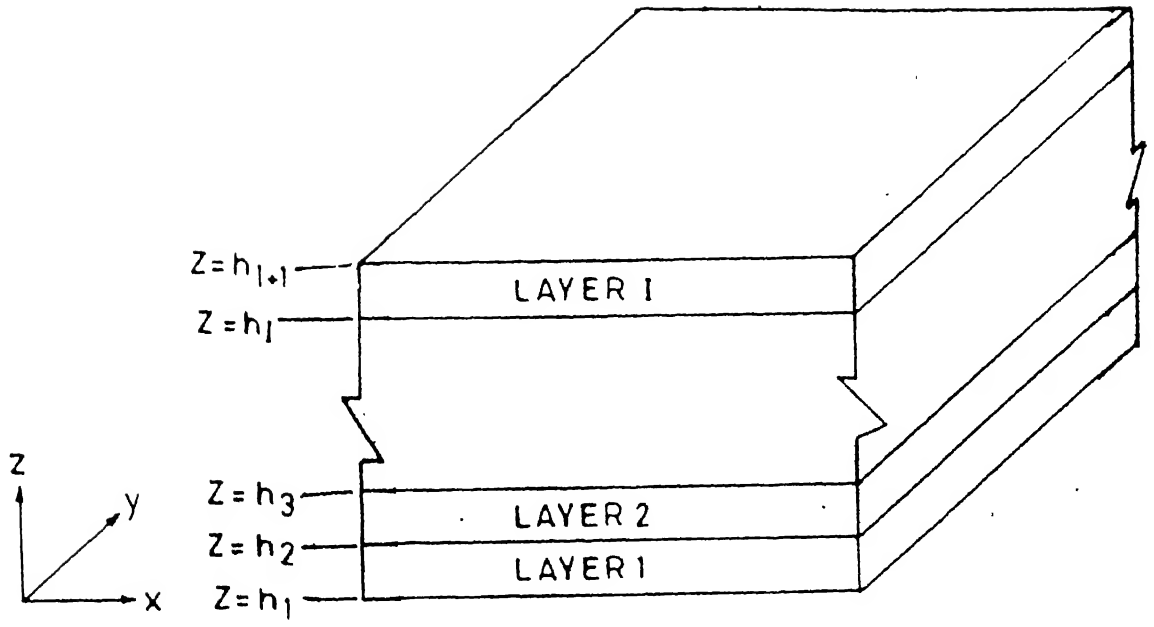

FIG. 3.1 GEOMETRY AND LAYER NUMBERING OF MULTILAYER PLATE ELEM

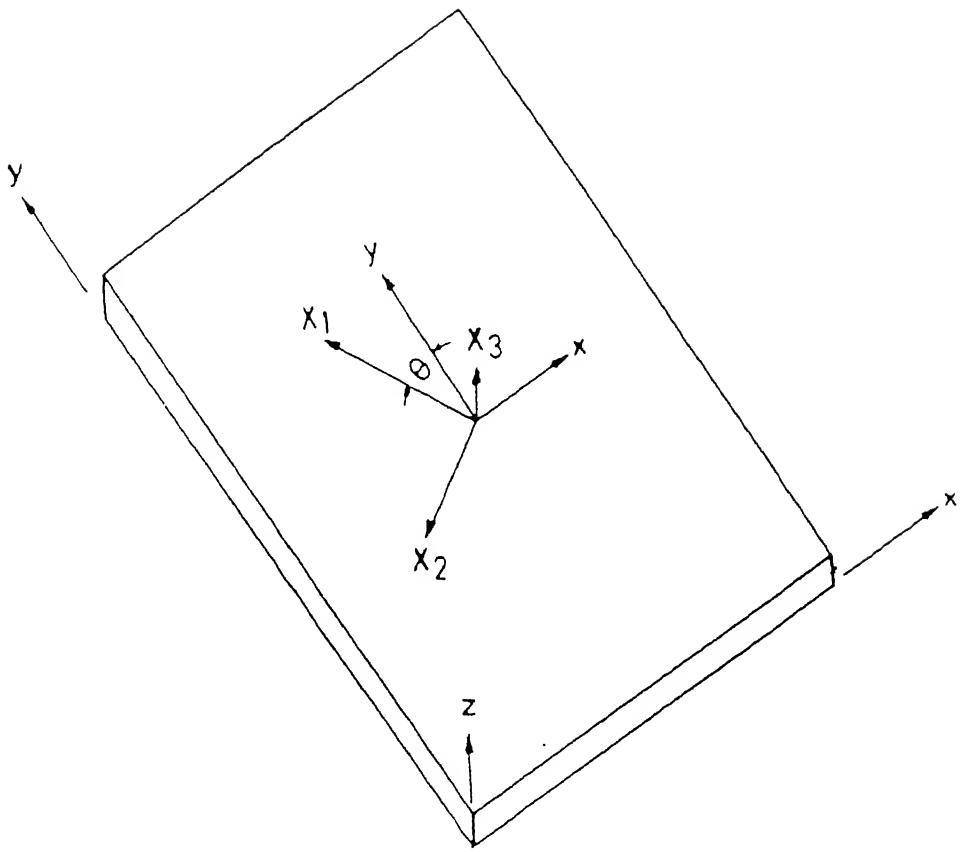

FIG.3.2. LAMINA WITH ITS PRINCIPAL MATERIAL AXES ORIENTED AT ANGL
θ WITH REFERENCE TO GLOBAL COORDINATE AXES.

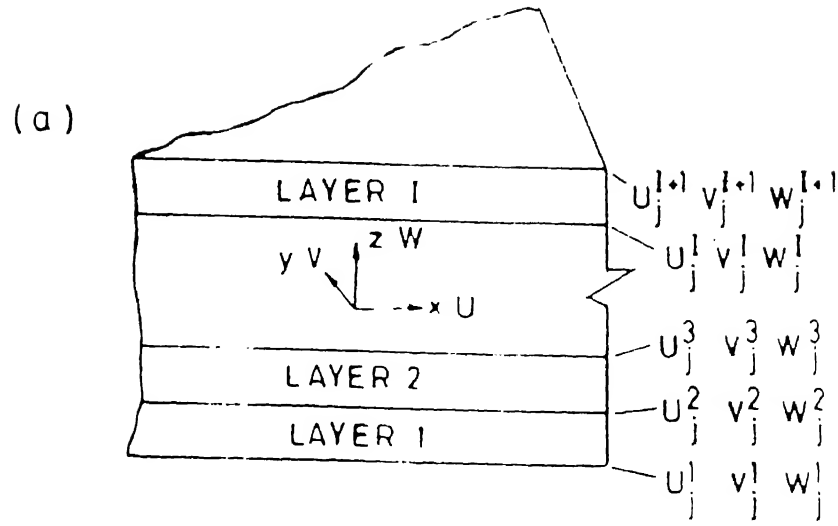

DISPALACEMENT DEGREE OF FREEDOM AT NODE J OF THE LAMINATE

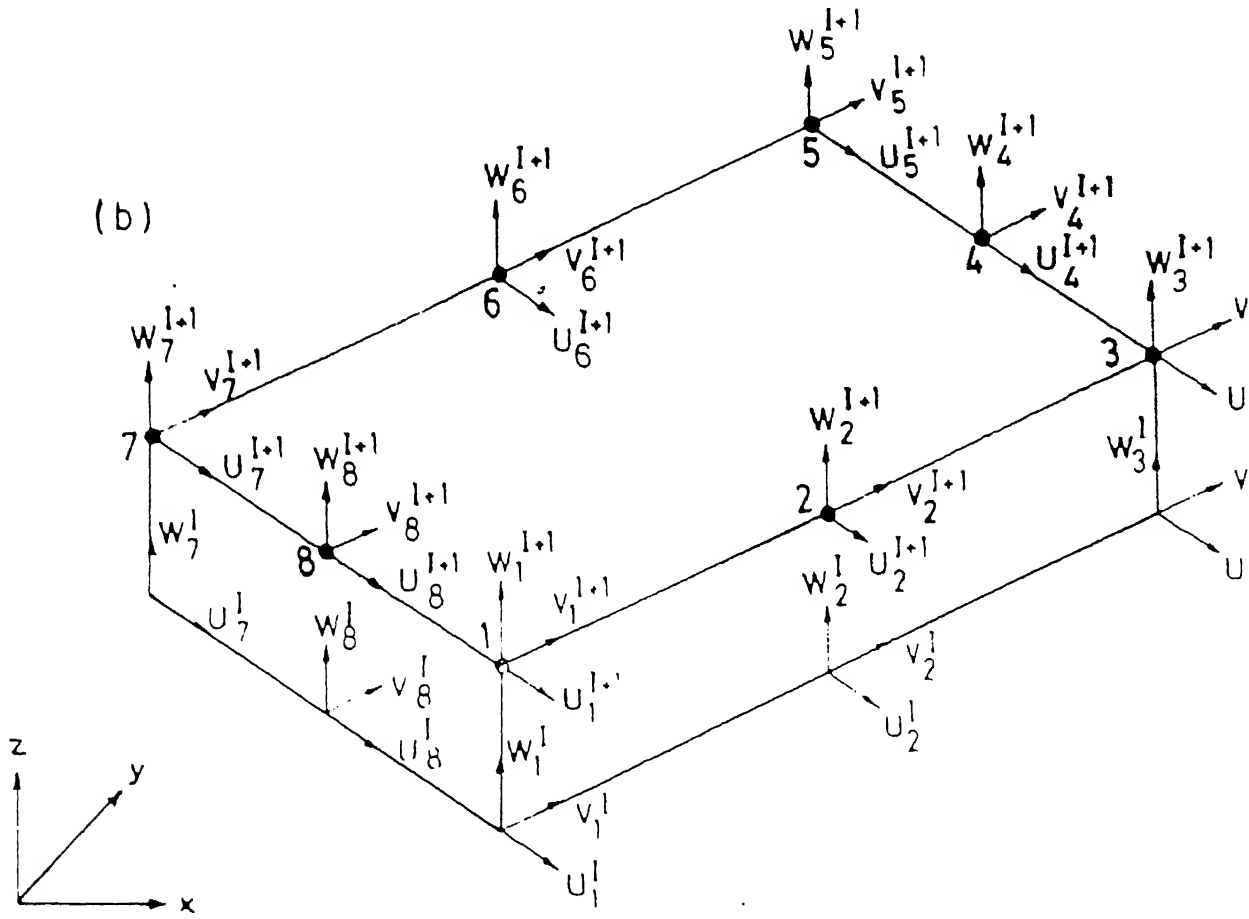

DISPALACEMENT DEGREE OF FREEDOM FOR LAYER I

FIG.3.3. DISPLACEMENT DEGREES OF FREEDOM

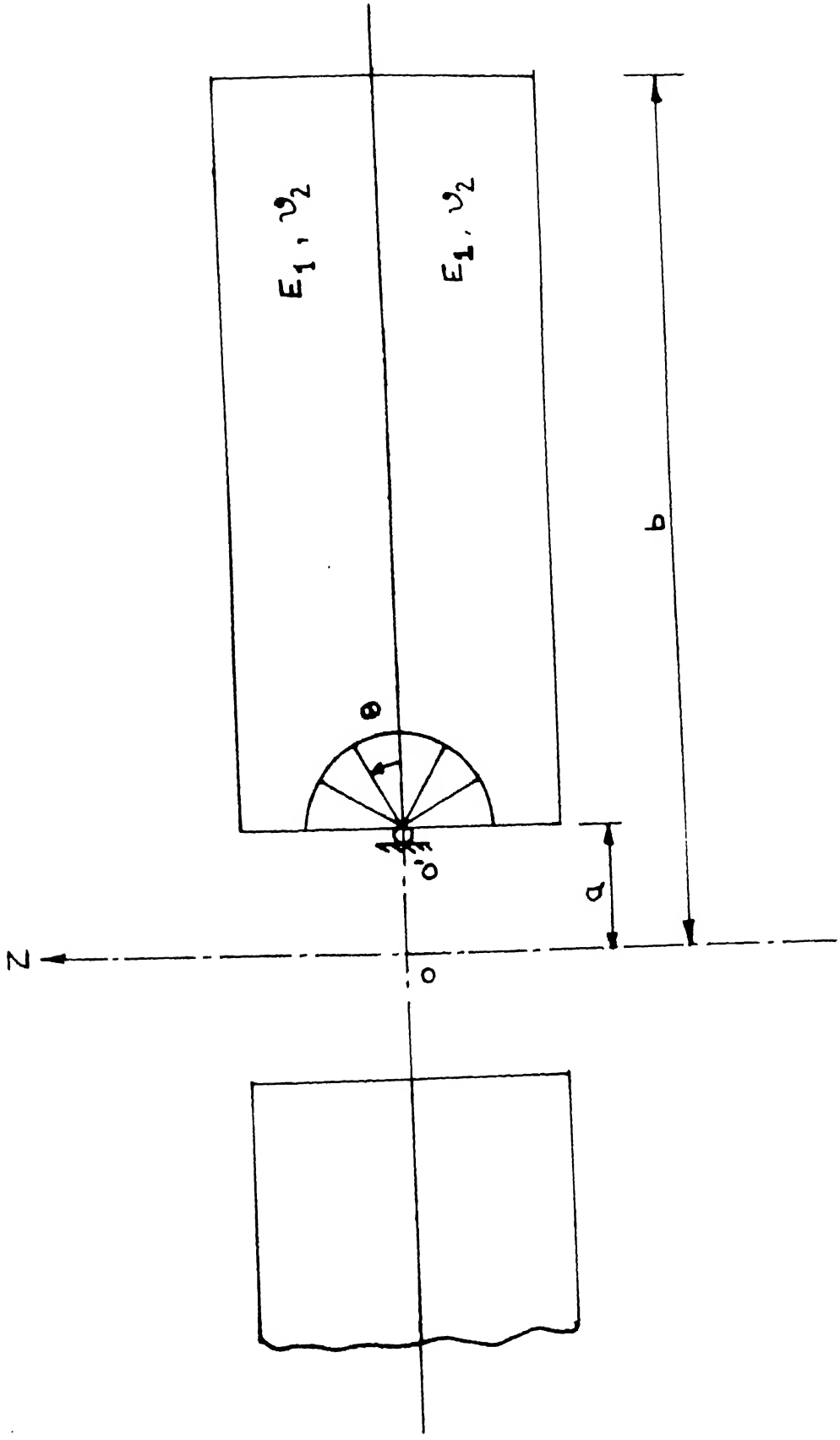

FIG.3.4. SINGULAR ELEMENTS AT HOLE BOUNDARY

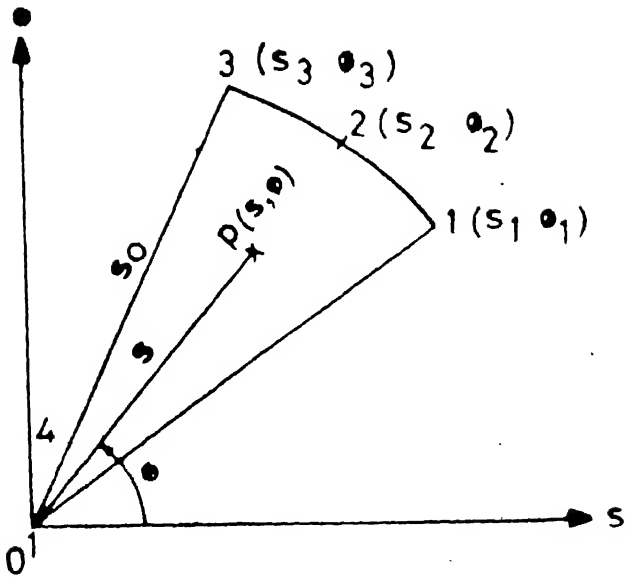

FIG.3.5. (a)

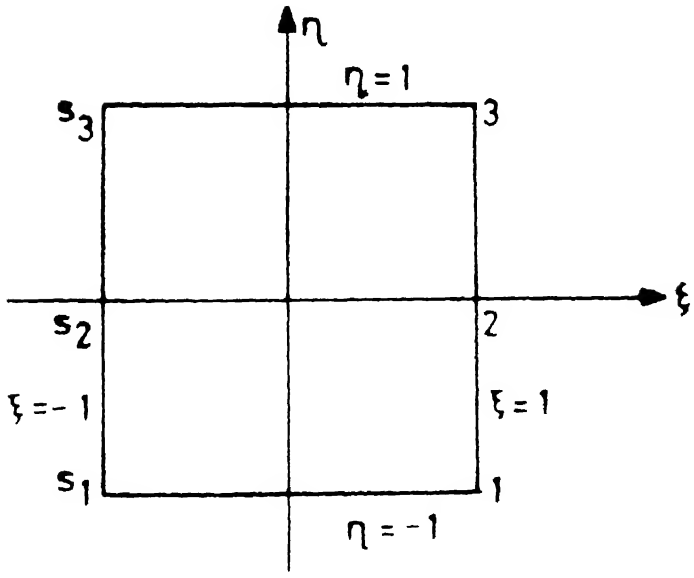

FIG.3.5. (b)

MAPPING FROM NATURAL COORDINATES ξ, η TO PHYSICAL COORDINATES

s AND θ

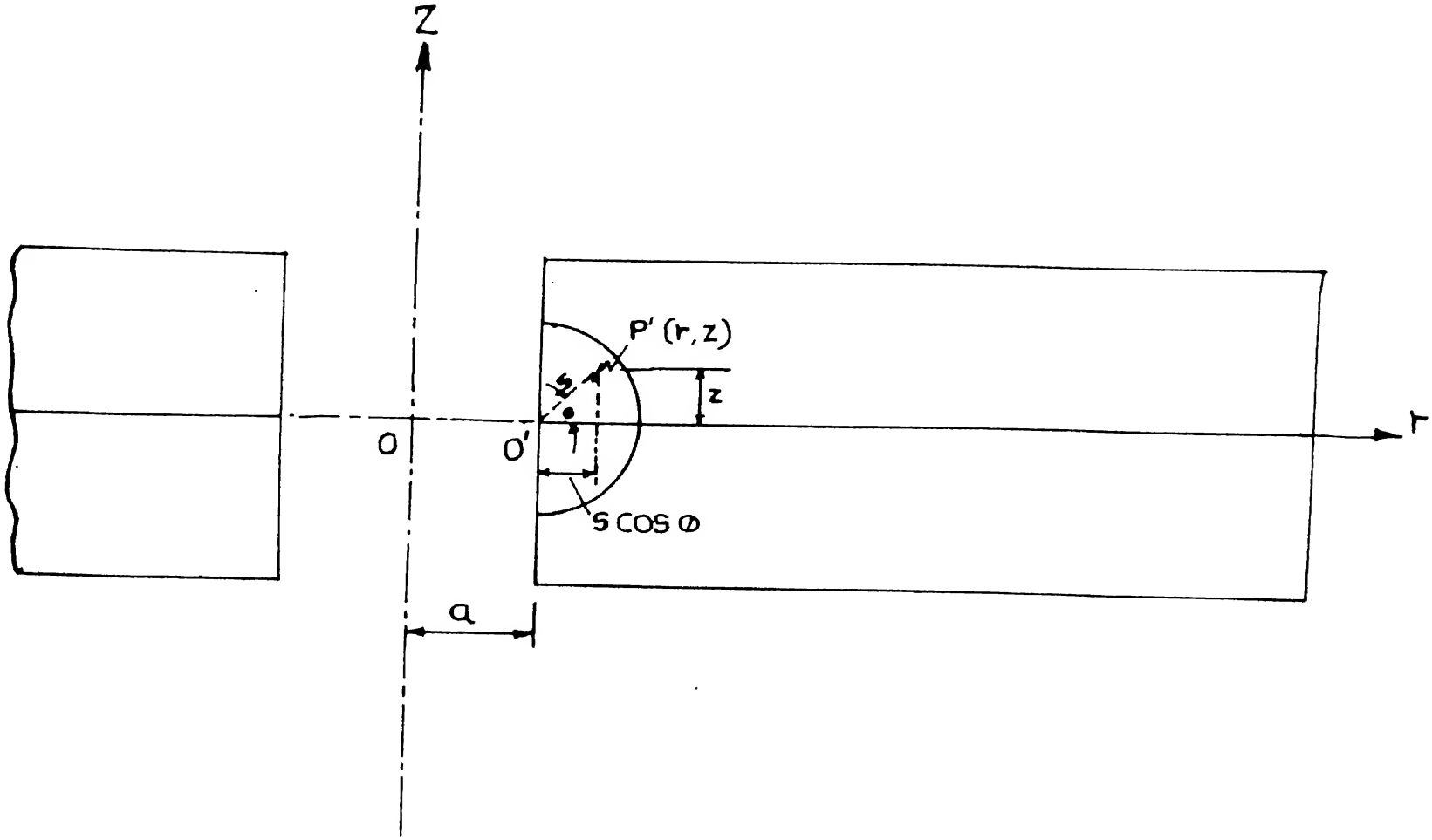

FIG.3.6. POSITION OF ANY POINT ON SECTOR w.r.t. AXISYMMETRIC AXIS

CHAPTER 4

RESULTS AND DISCUSSIONS

This chapter presents the free-edge stresses in laminated composite plates subjected to a far field uniform strain ε_y. The analysis has been carried out using hybrid finite element and singular hybrid element approach as discussed in the previous chapters. Results show the effectiveness of the singular hybrid elements near the boundary. Two geometries have been considered for analysis:

1. A symmetric crossply laminate with a central circular hole with $[0/90]_S$ and $[90/0]_S$ configurations.
2. A symmetric crossply laminate with a central square hole with $[0/90]_S$ configuration.

Details of the geometric and material data has been given in chapter II.

4.1 Interlaminar Stresses Near the Circular Hole Boundary in Symmetric Composite Laminate

As discussed in chapter-I, there are situations where the composite laminates have holes, cut outs etc., which are a possible site for delamination. The inter-laminar stresses near the free edge of a circular hole in symmetric $[0/90]_S$ and $[90/0]_S$ laminates have been investigated.

Figure 4.1 shows a finite element discretization of the laminated composite plate with a central circular hole used in the present analysis. The laminate is subjected to a uniform far field strain in y-direction. As may be observed, only $1/8^{th}$ of the plate has been modelled due to the

symmetries of the plate about the x,y and z axes. The mesh is finer near the hole boundary and has a total of 85 elements. The elements are hybrid in nature with 67 β's per ply (or 119 terms in all). As discussed earlier, only the elements near the hole boundary have been treated as singular hybrid elements with an additional three terms to model singularity. The singular hybrid finite element analysis has also been performed using a finer mesh having total of 170 elements as shown in figure 4.2.

As a first step in formulating hybrid elements, the value of singularity of stresses near the hole boundary at the interface has been determined as explained in sec. 3.3, Fig 4.3 shows the variation of singularity values with the angle θ. As can be seen, the severity of singularity is the highest at $\theta = 0^{\circ}$ and $\theta = 90^{\circ}$ as the material properties of the plies differ maximum at these two locations. At $\theta = 45^{\circ}$, the reduced axisymmetric material properties do not differ and hence the singularity value is zero. These singularity values have been used in the construction of the stress terms in addition to the cubic variation, for the elements near the hole boundary.

In what follows, these stresses have been normalised with a factor S_g as given by

$$S_g = 302\ u_0/h \text{ Mpa}$$

$$S_g = 43 \times 10^9\ u_0/h \text{ Psi}$$

Fig 4.4 - 4.6 show the interface normal stress, σ_z, near the hole boundary obtained by using a coarse mesh of 85 elements. The variation is shown along radial lines at $\theta = 0^{\circ}$, $\theta = 45^{\circ}$ and $\theta = 90^{\circ}$. In the same figures, curves are also shown as obtained by Chahande(1989) without incorporating the singular elements and those of Raju and Crews(1982) obtained by

displacement formulation employing a very fine mesh(19000 degrees of freedom). As can be observed, the results with singular elements are much closer to those obtained by Raju and Crews(1982). The interface normal stress σ_z will become negligible far away from the hole. However, in the present analysis, the rate of decay is a little less. This can be attributed to the coarse mesh away from the hole. These graphs prove beyond doubt the fact that the inclusion of the singular terms for the elements adjacent to the hole boundary improves the accuracy markedly and the value of the singularities in a simple axisymmetric analysis may be effectively used.

Figs.(4.7 - 4.9) show the plots of interface normal stress along the radial lines at $\theta = 0^o$, $\theta = 45^o$ and $\theta = 90^o$. They show the results obtained for a fine mesh with 170 elements (fig. 4.2) without singular elements and with singular elements adjacent to the hole boundary. It can be seen that the results are exactly same in the far field region but are different in terms of magnitude near the hole boundary. In the case of variation along $\theta = 0^o$ line the present analysis shows very negligible interlaminar stress σ_z as is expected. However, at the free edge, there is a complete reversal in the nature of the stress. Comparing with Raju and Crews results, the compressive nature as determined by the analysis with singular elements is correct. Along $\theta = 45^o$ the stresses are compressive near the free edge and for $\theta = 90^o$, they are tensile. It is worth noting that this is a possible location for delamination initiation and growth.

Fig.4.10 shows the variation of the transverse τ_{rz} shear stress in the radial direction along $\theta = 0^o$, $\theta = 45^o$ and $\theta = 90^o$. These stresses are zero at the hole boundary all in the three directions. This is due to the correct enforcement of the $\tau_{rz} = 0$ boundary condition during the

derivation of the singular terms which is not apparent in the results by Raju and Crews.

Figures 4.11 shows the hoop stress σ_θ variation near the hole boundary in the thickness direction at $\theta = 0^o$, $\theta = 45^o$ and $\theta = 90^o$. One feature worth noting is that this stress shows a distinct dicontinuity at the interface.

From the σ_z through thickness distribution shown (fig 4.12), the following can be observed. The interlaminar stresses σ_z have a large slope discontinuity at the interface as compared to the discontinuity observed by Raju and Crews. This may be attributed to the fact that the interlayer traction continuity has been enforced in the present formulation.

Fig 4.13 and Fig 4.14 show the variation of σ_z and τ_{rz} respectively in the three radial directions for the crossply laminate of the $[90/0]_s$ configuration. Except for the 0^o direction, these stresses have changed in nature as compared to the $[0/90]_s$ case. This shows that the possibility of delamination is also reversed.

Figs 4.15 and 4.16 show the through thickness variations of the hoop stress σ_θ and σ_z for the $[90/0]_s$ configuration. As in case of the $[0/90]_s$ results, the σ_θ distribution shows a discontinuity at the interface, while the σ_z distribution shows a smooth variation with large slope.

4.2 Edge Stresses Near the Square Hole Boundary in Symmetric Composite Laminate.

Similar to analysis of edge stresses near a circular hole in a symmetric laminate, singular hybrid finite element method analysis is

carried out in the case of a $[0/90]_S$ laminate with a square hole. The laminate geometry and material properties are the same as in the previous case. The finite element discretization of the laminate is shown in figure 4.17. The mesh is made finer near the hole and has a total number of 85 elements. Analysis was also carried out using a fine mesh having 170 elements (fig.4.18). However, there is one difference between the employment of singular terms in the construction of the hybrid elements adjacent to the hole. As the hole boundaries are straight (parallal to the x or y axes), the singularity is taken to be constant and equal to the value at either 0° or 90°.

The radial variation of the interlaminar stress σ_z and interlaminar shear stress τ_{rz} are shown in figs.4.19 - 4.20. These stresses have been plotted along the $\theta = 0^{\circ}$, $\theta=45^{\circ}$ and $\theta = 90^{\circ}$. Here the normal stress σ_z at $\theta=0^{\circ}$ is negligible as was in the case of the circular hole problem, whereas it has significant positive value near $\theta = 45^{\circ}$ in contrast to the previous problem. At $\theta = 90^{\circ}$, it follows the same trend as in the previous case and has a significant positive value. These values seem to be much more than those in case of circular hole. However overall variation is the same. Thus square hole seems to have more tendency for delamination.

The through thickness variation of the hoop stress σ_θ and interlaminar normal stress σ_z are shown in figs.4.21 - 4.22. The hoop stress σ_θ as in the previous case, shows a distinct discontinuity at the interface but with a very high magnitude of the stress. Th interlaminar stress σ_z, due to the reasons discussed earlier, does not show discontinuity at the interface.

It can be further concluded that the presense of significant

interlaminar normal stresses and interlaminar shear stresses near the free edge, may act in conjunction, leading to mixed modes of failures.

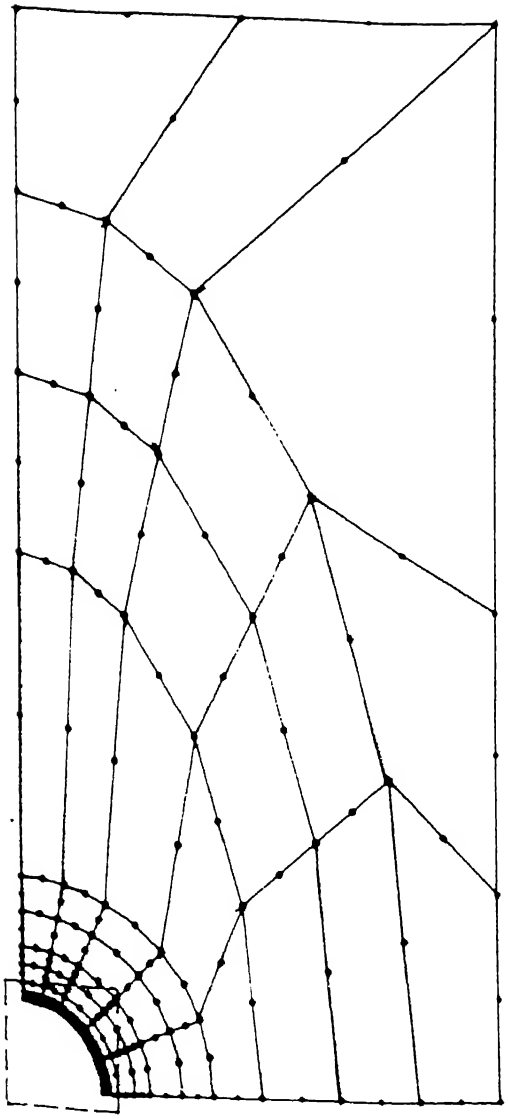

NO. OF ELEMENTS = 85

NO. OF NODES = 300

NO. OF TOTAL DEGREES OF FREEDOM = 2700

R = 5" ; b = 30" ; 1 = 60°

THICKNESS (PLY) = 0.25"

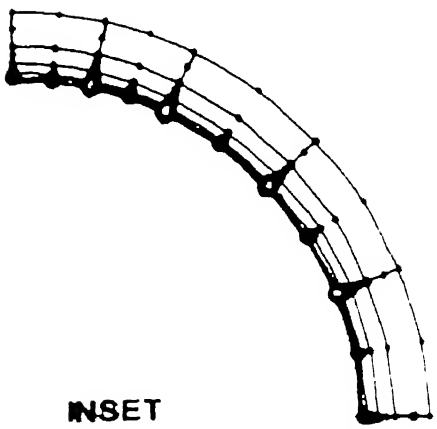

INSET

FIG.4.1 FEM DISCRETIZATION OF LAMINATE PLATE WITH CIRCULAR HOLE

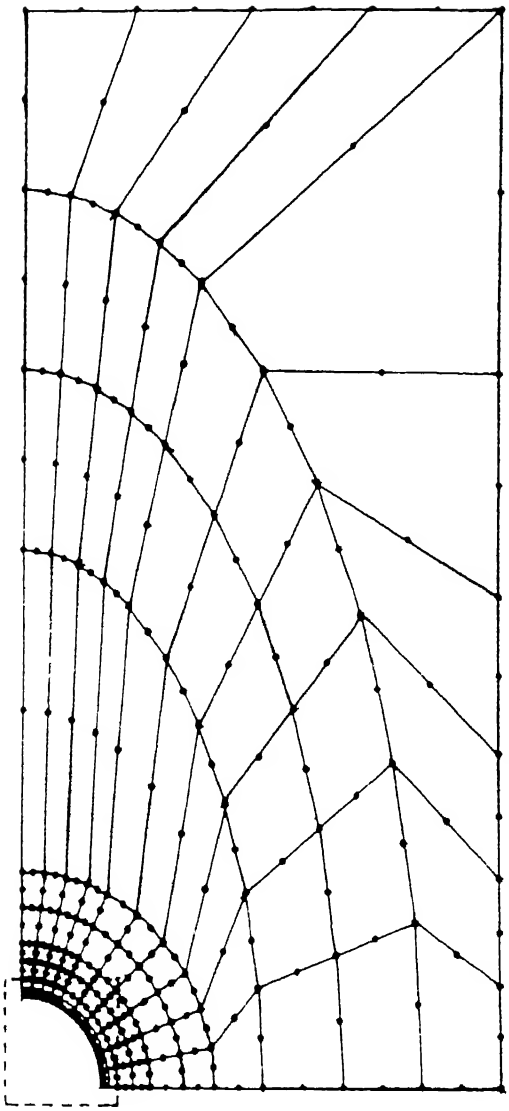

NO. OF ELEMENTS = 170

NO. OF NODES = 565

NO. OF TOTAL DEGREES OF FREEDOM = 5065

R = 5" ; b = 30" ; l = 6

THICKNESS (PLY) = 0.25"

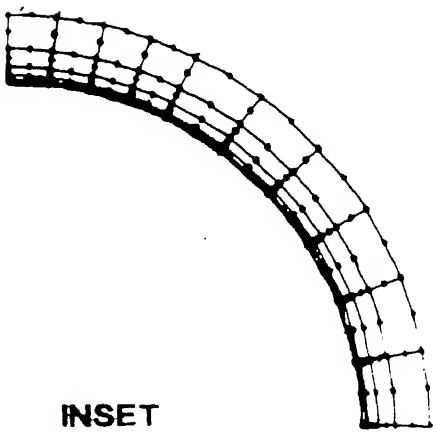

INSET

FIG.4.2. FEM DISCRETIZATION OF LAMINATE PLATE WITH CIRCULAR H

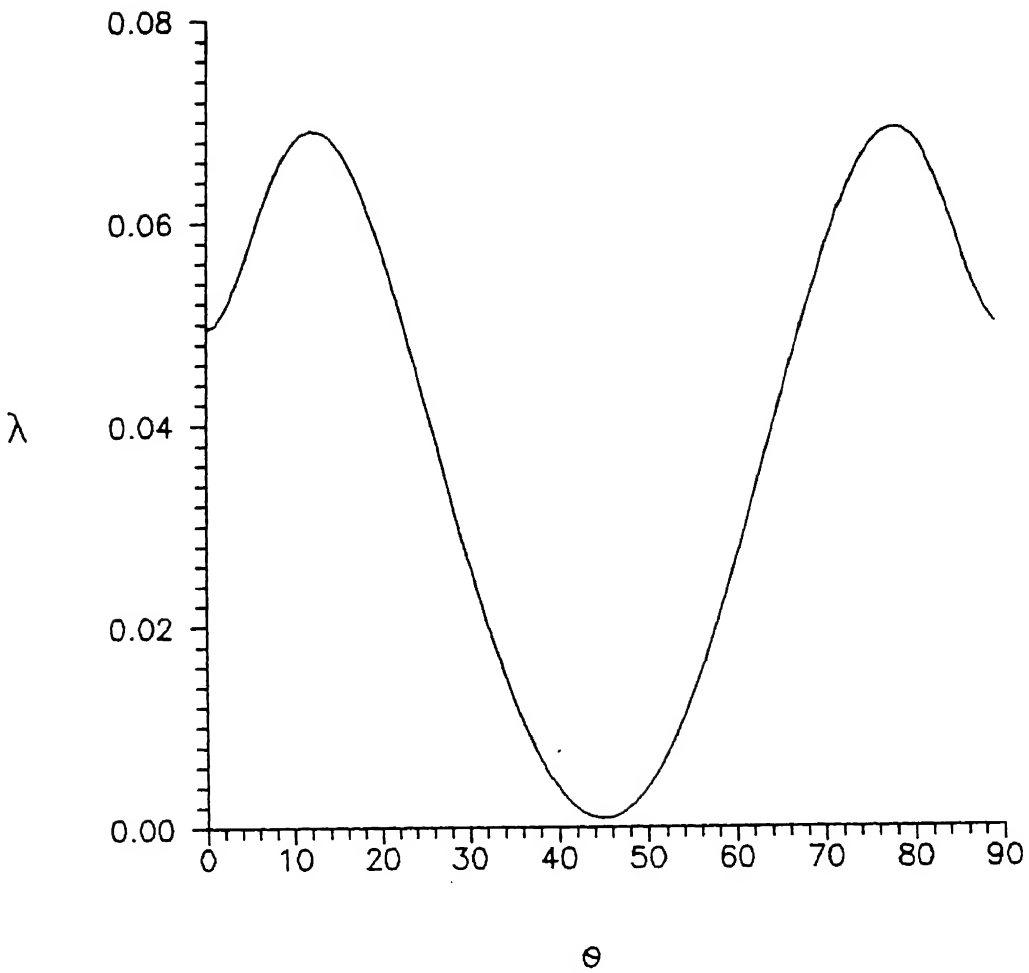

Fig.4.3 Angular variation of Power of Singularity

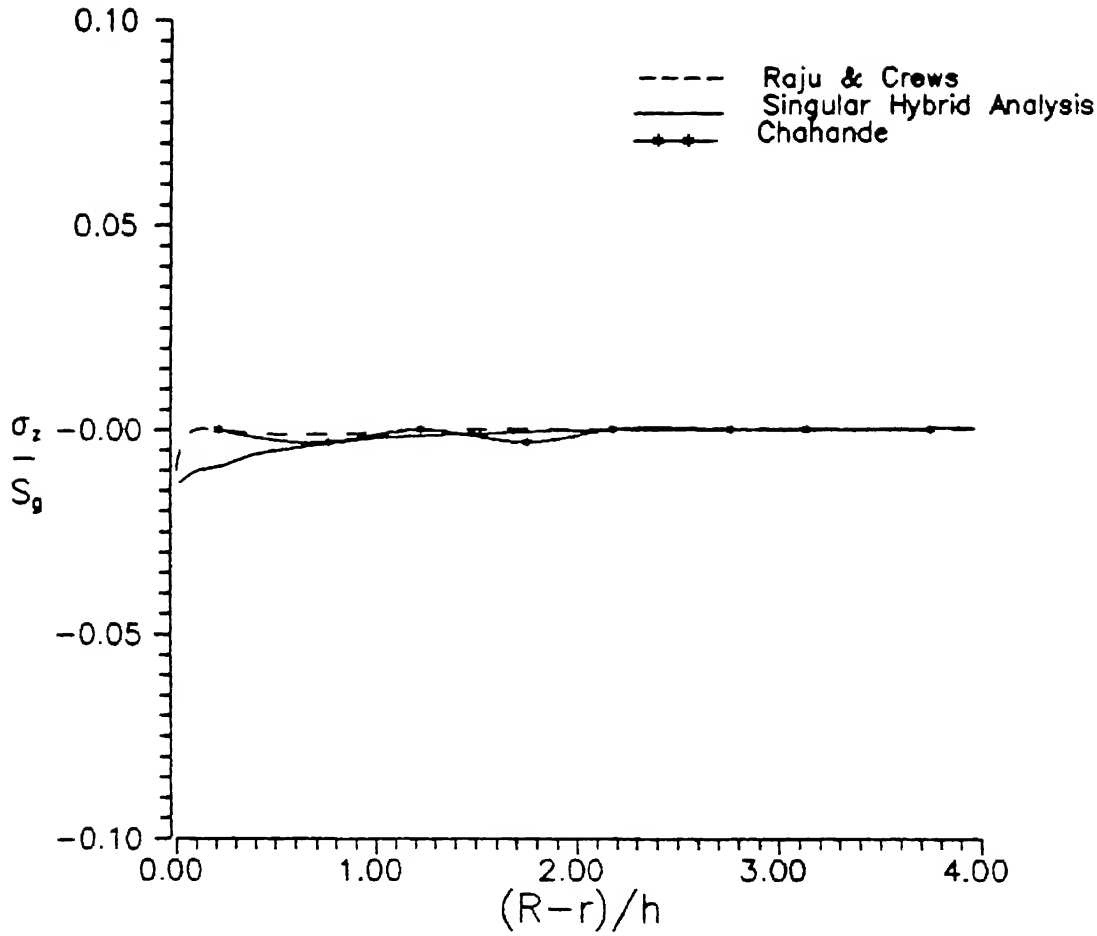

Fig.4.4 σ_z radial distribution for 0/90 laminate with circular hole (85 elements) − $\theta = 0°$

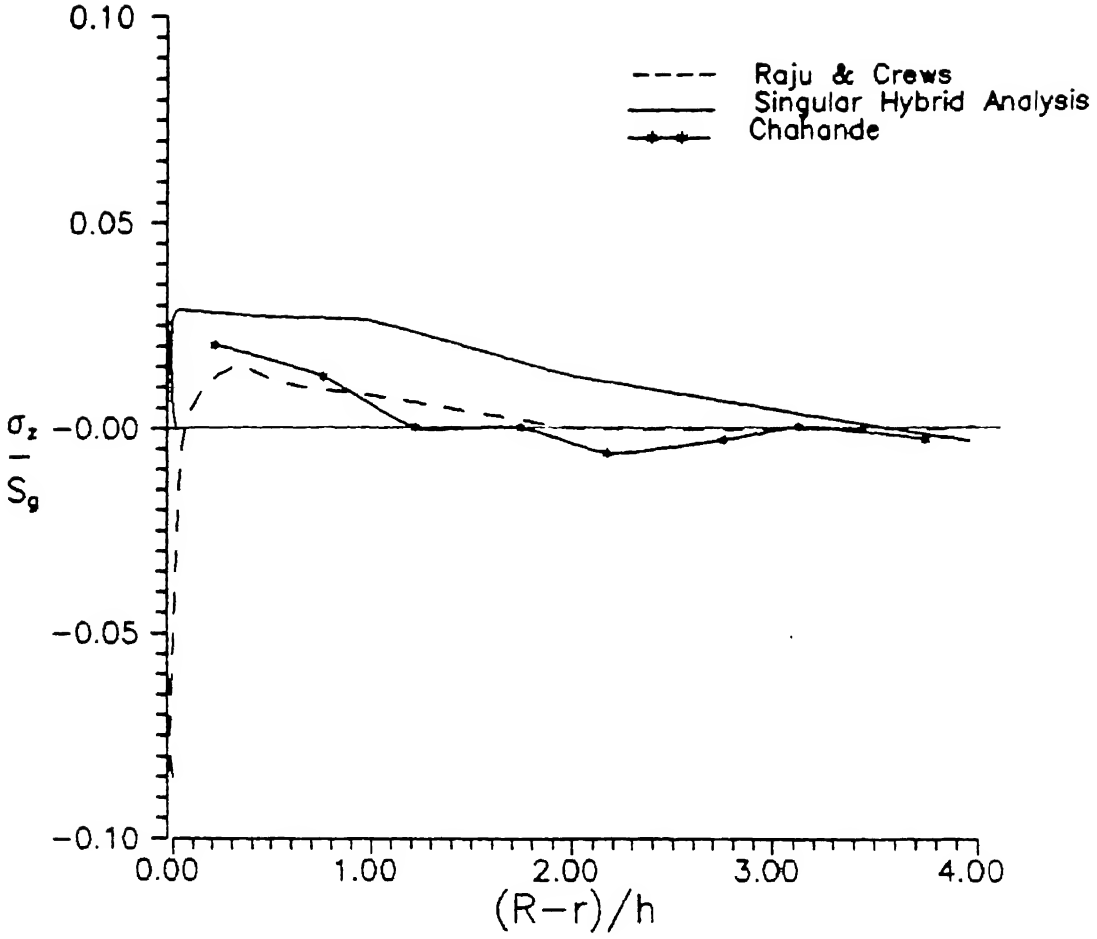

Fig.4.5 σ_z radial distribution for 0/90 laminate with circular hole (85 elements) − $\theta = 45°$

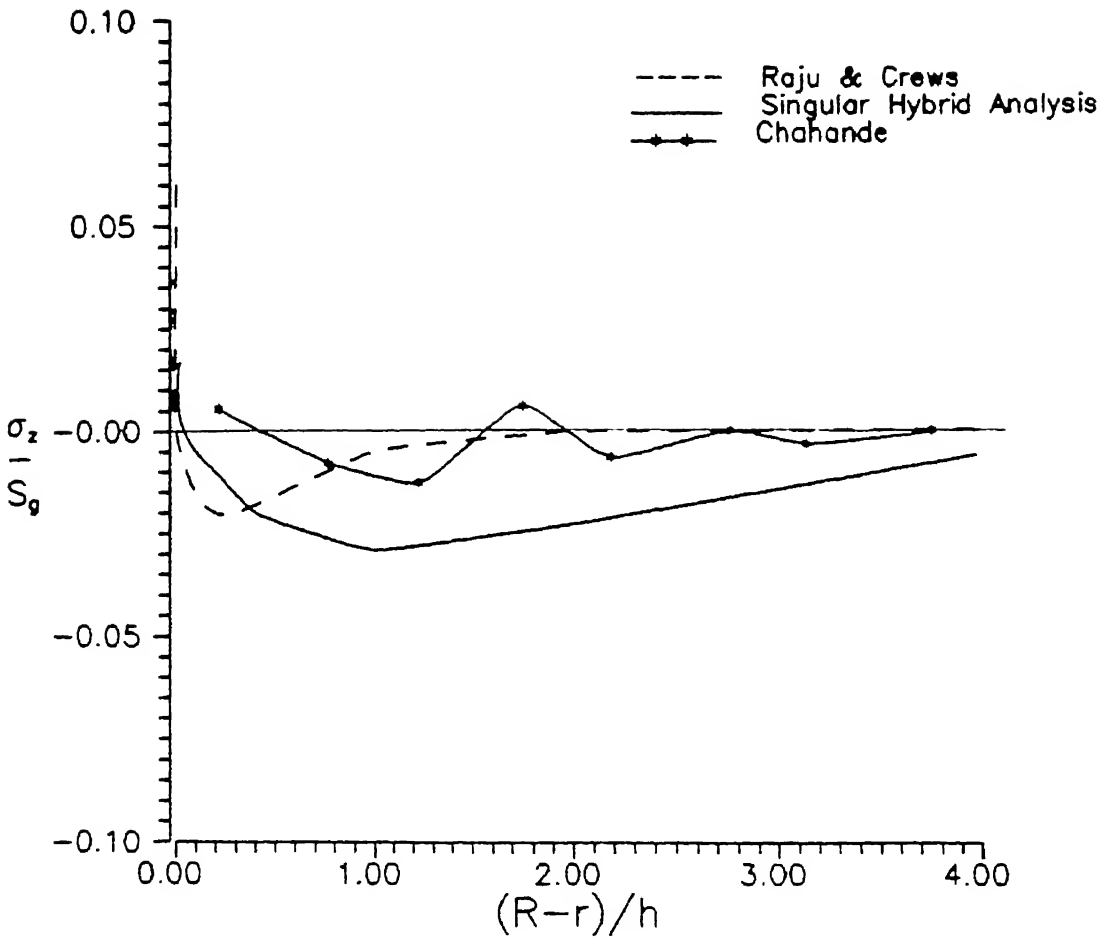

Fig.4.6 σ_z radial distribution for 0/90 laminate with circular hole (85 elements) − $\theta = 90°$

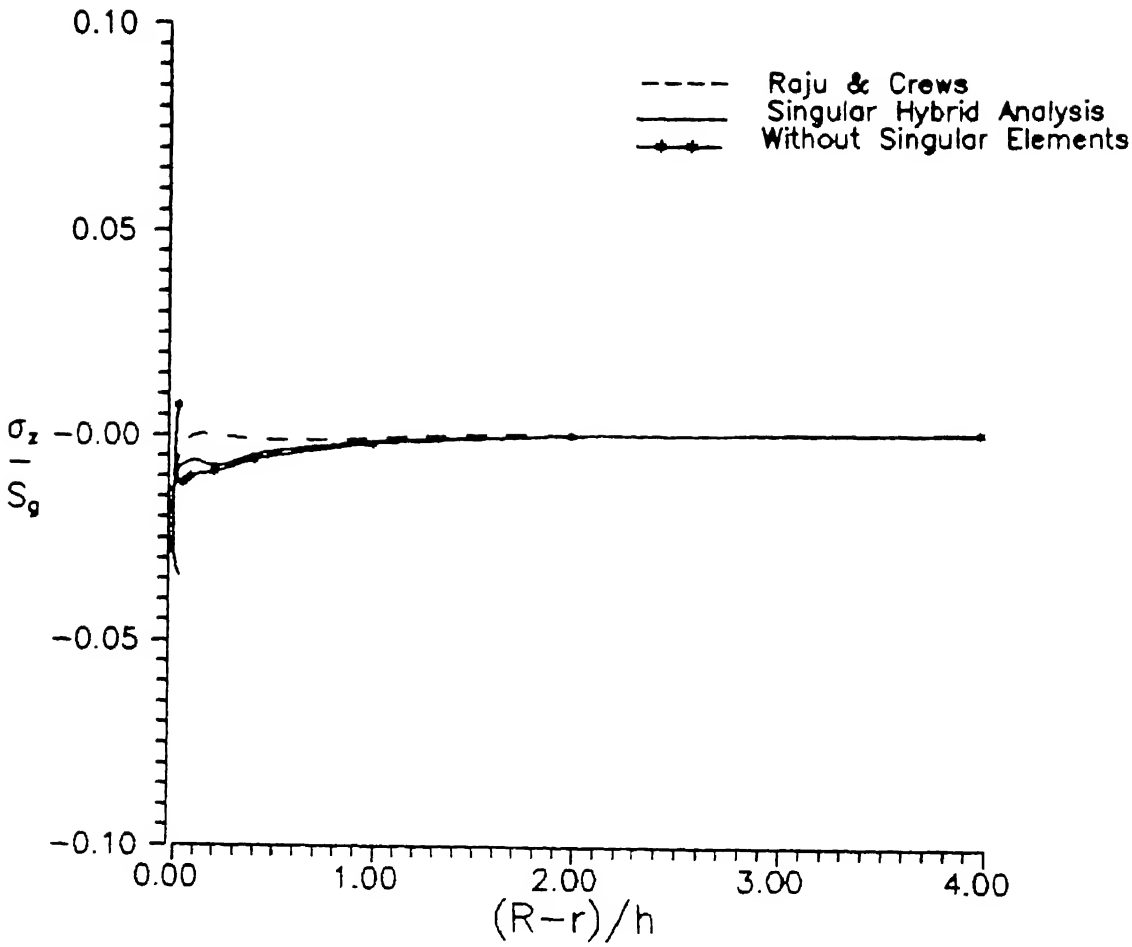

Fig.4.7 σ_z radial distribution for 0/90 laminate with circular hole (170 elements) − $\theta = 0°$

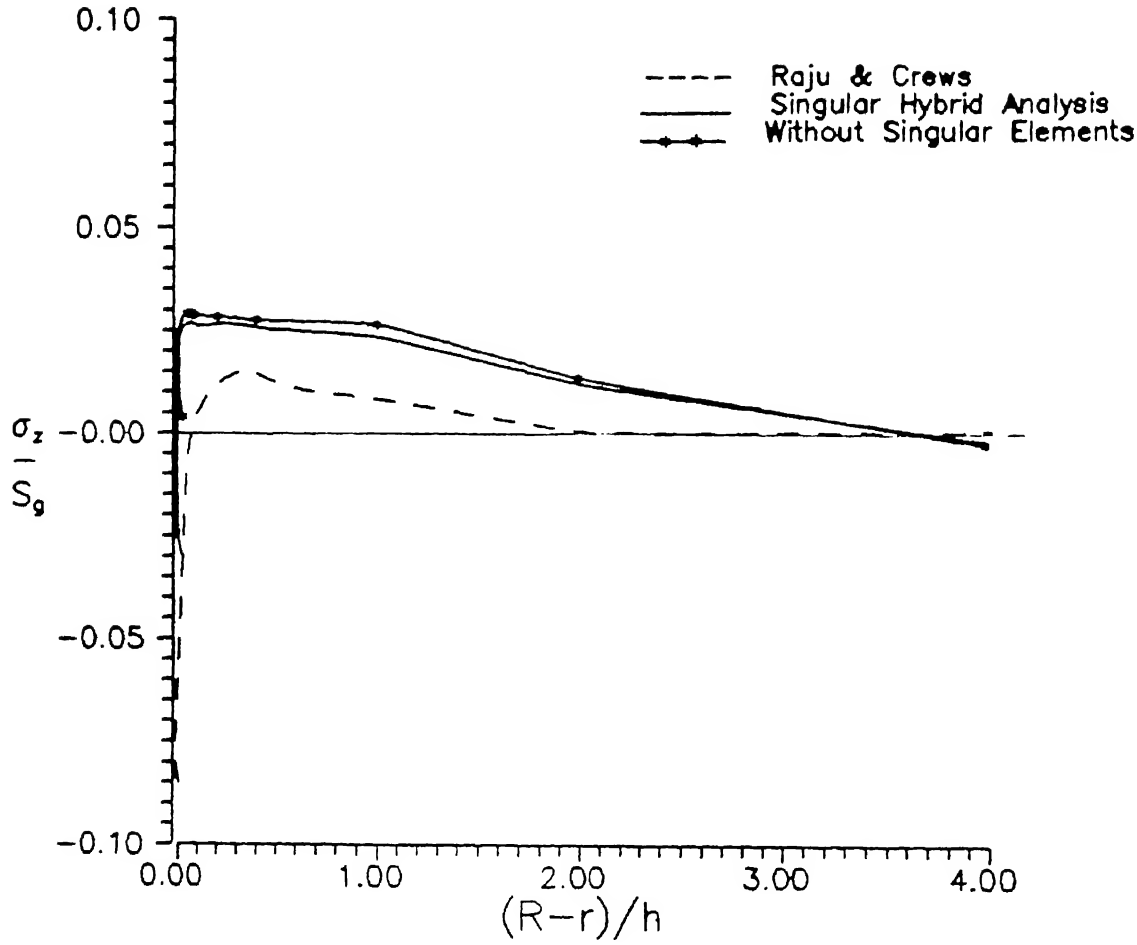

Fig.4.8 σ_z radial distribution for 0/90 laminate with circular hole (170 elements) – $\theta = 45°$

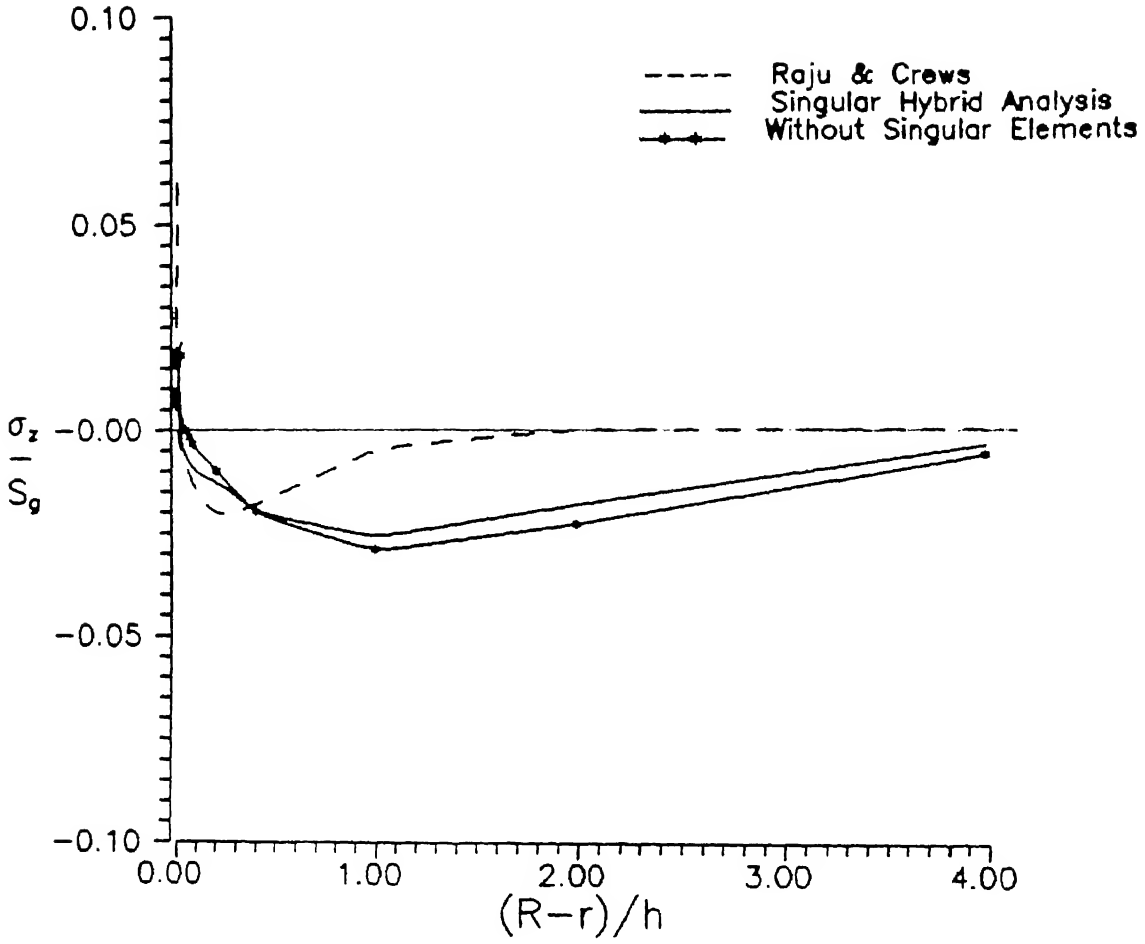

Fig.4.9 σ_z radial distribution for 0/90 laminate with circular hole (170 elements) – $\theta = 90°$

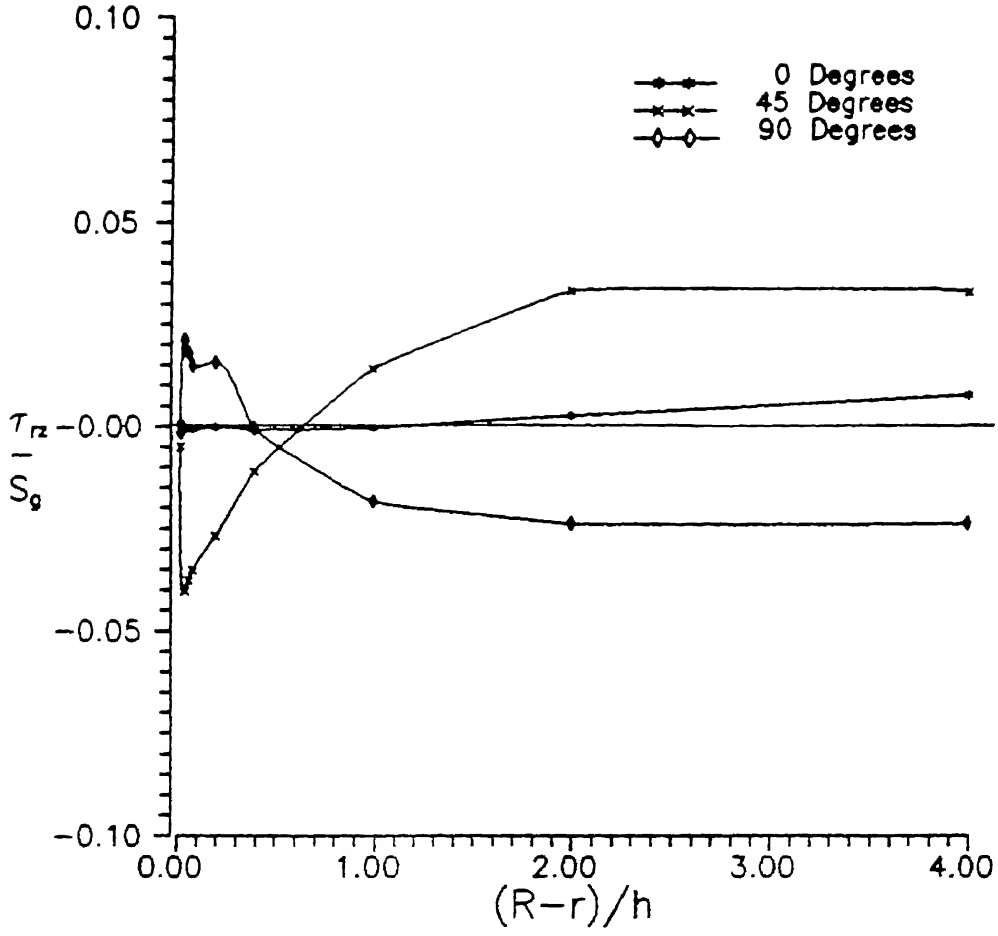

Fig.4.10 τ_{rz} radial distribution for 0/90 laminate with circular hole (170 elements)

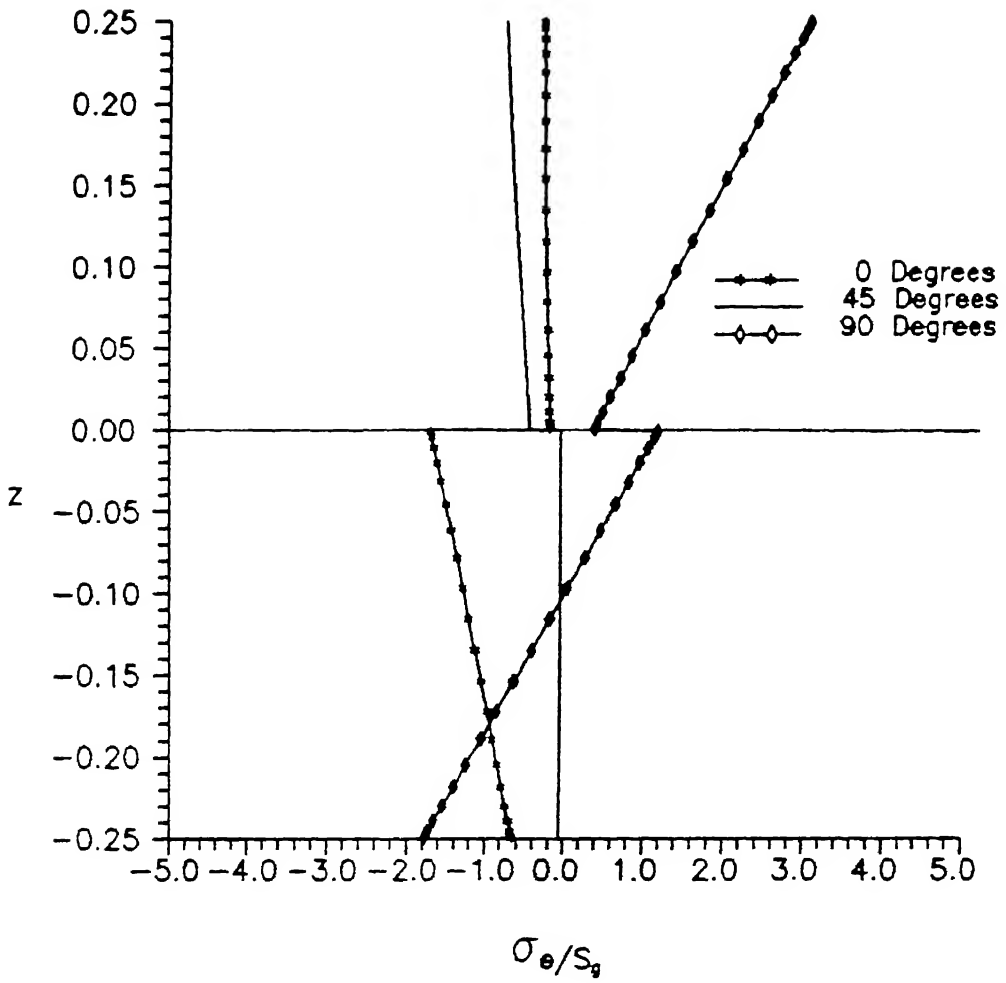

Fig.4.11 σ_θ through thickness distribution for 0/90 laminate with circular hole (170 elements)

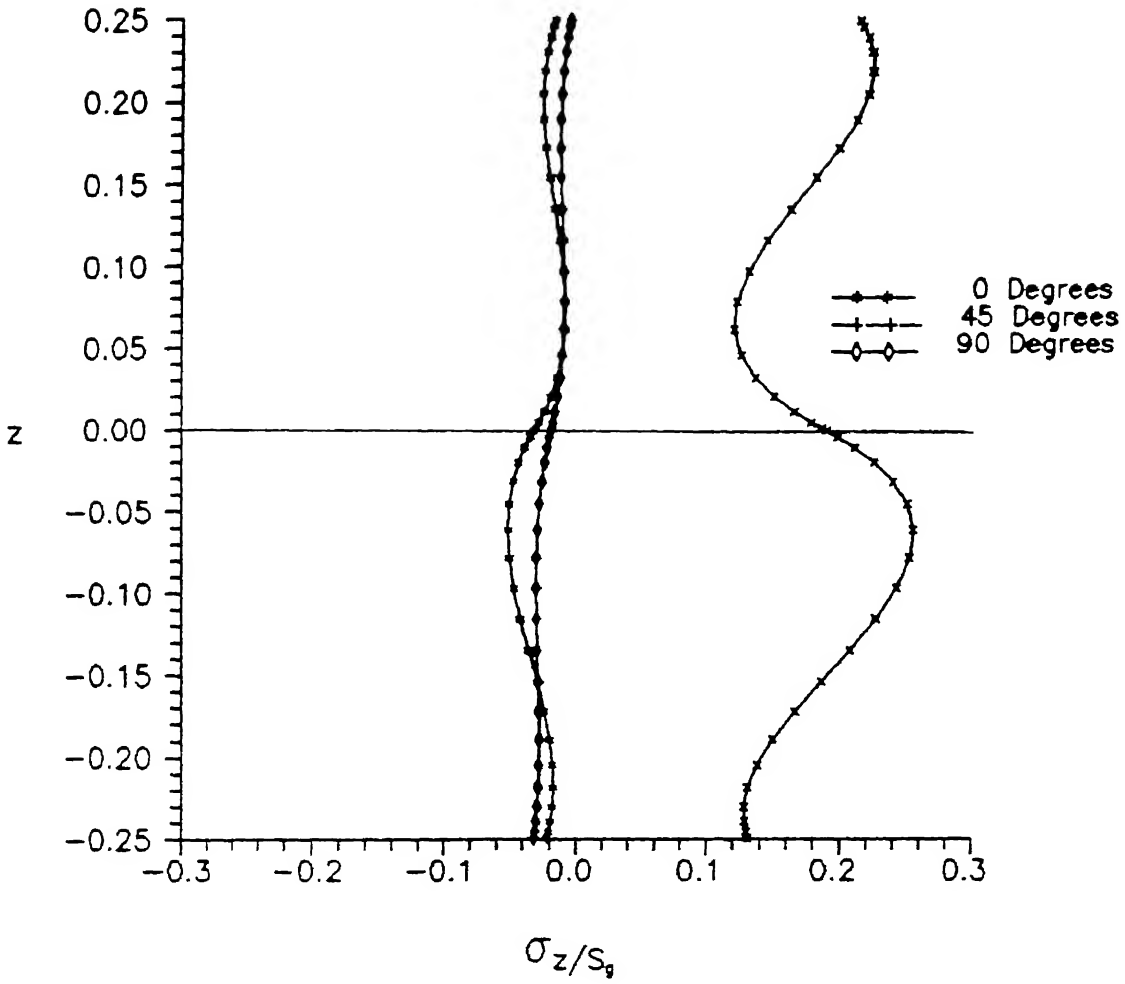

Fig.4.12 σ_z through thickness distribution for 0/90 laminate with a circular hole (170 elements)

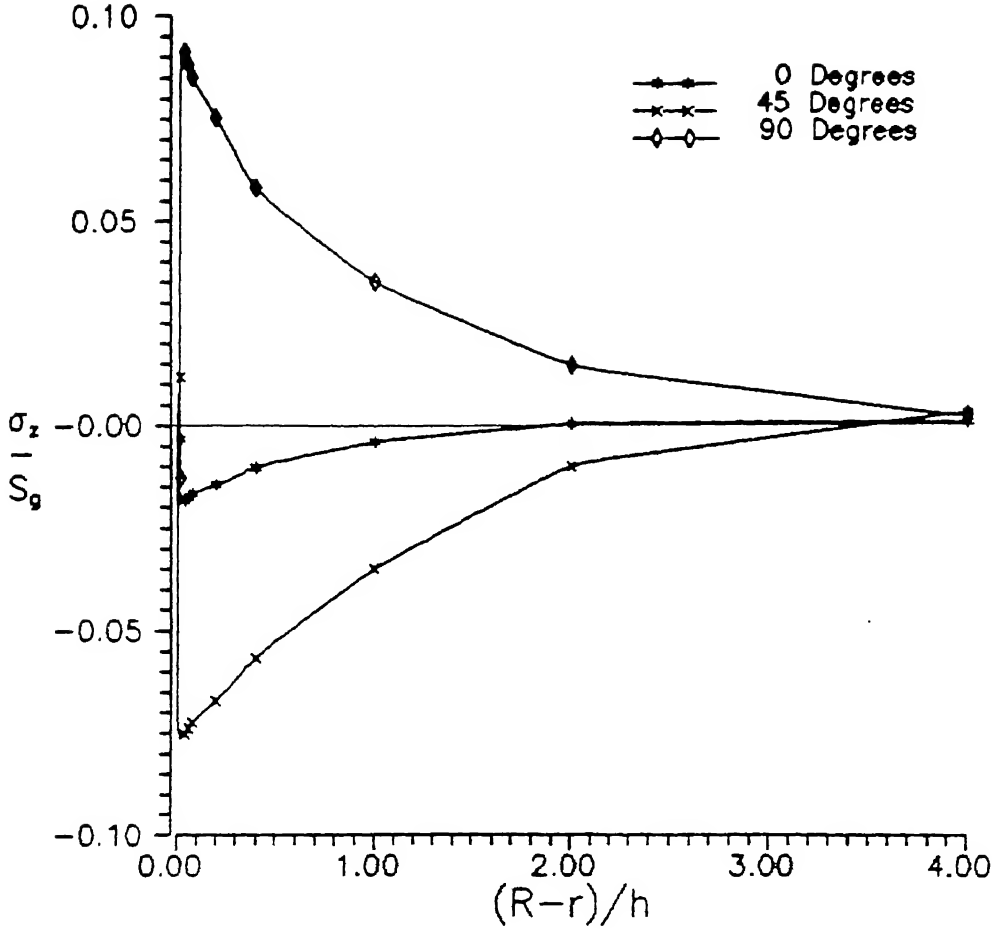

Fig.4.13 σ_z radial distribution for 90/0 laminate with circular hole (85 elements)

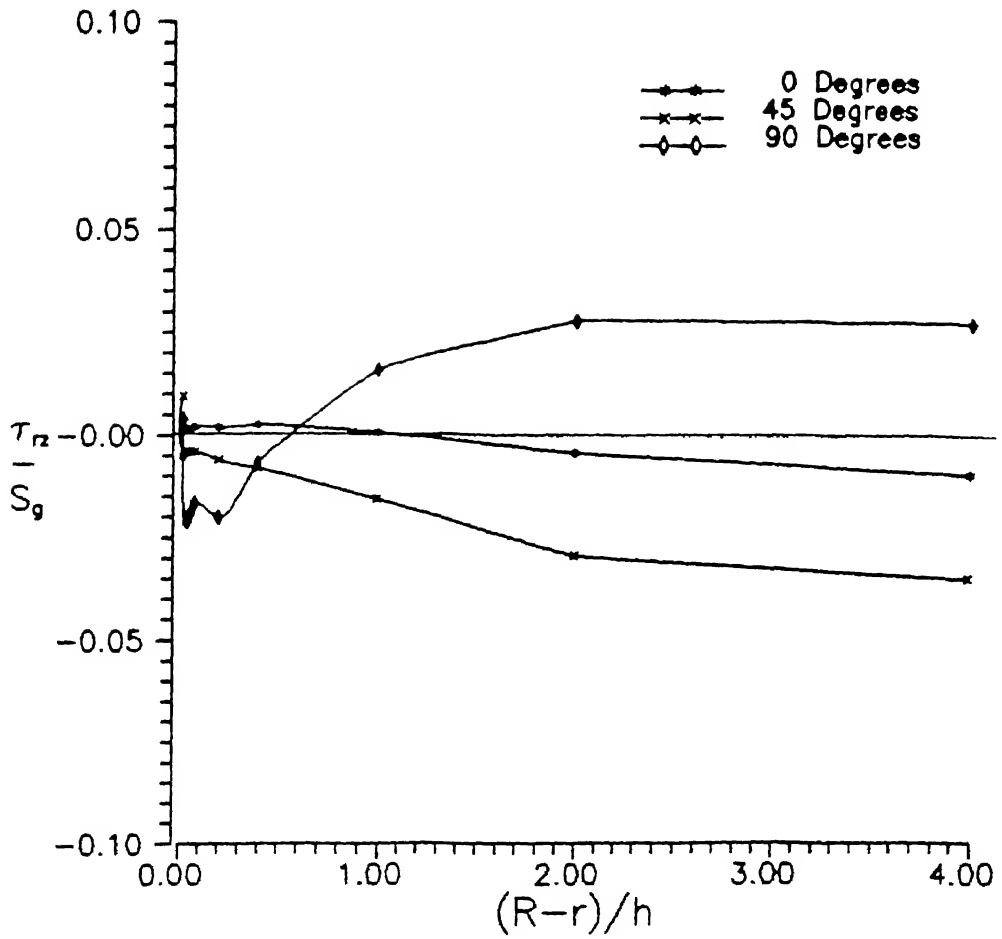

Fig.4.14 τ_{rz} radial distribution for 90/0 laminate with circular hole (85 elements)

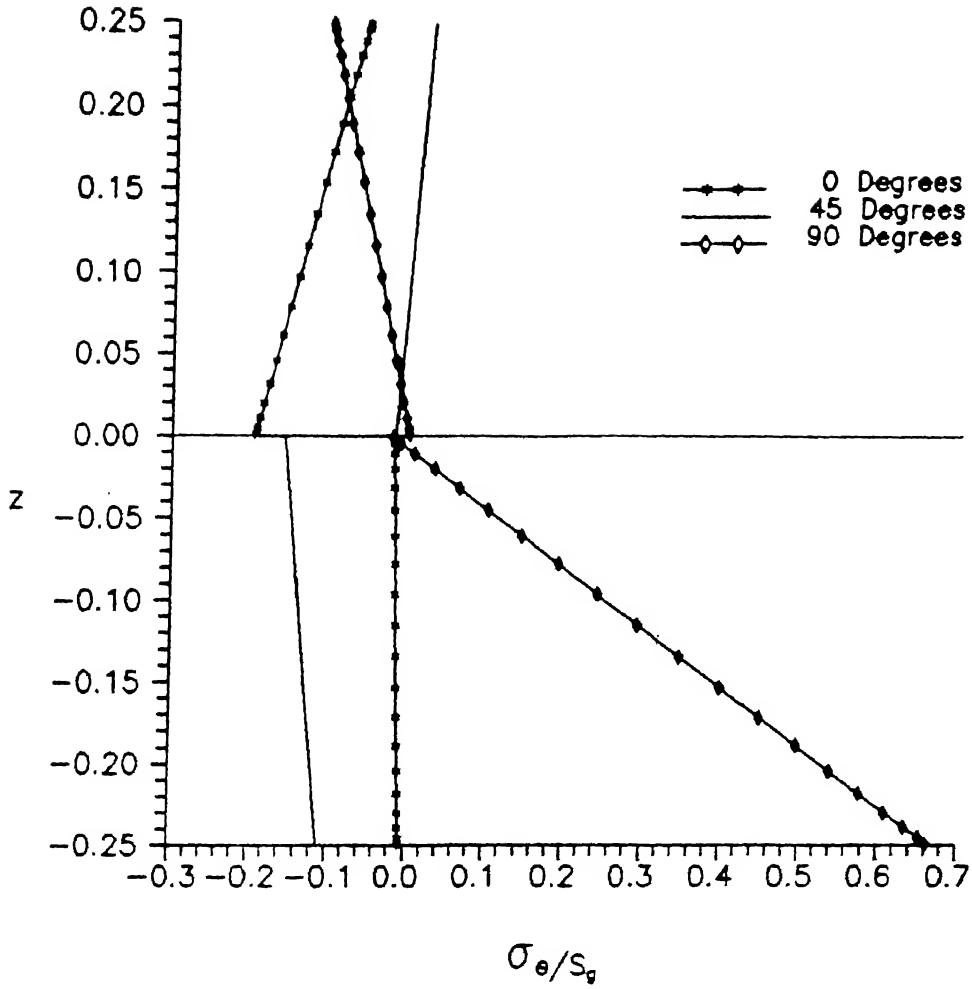

Fig.4.15 σ_{θ} through thickness distribution for 90/0 laminate with circular hole (85 elements)

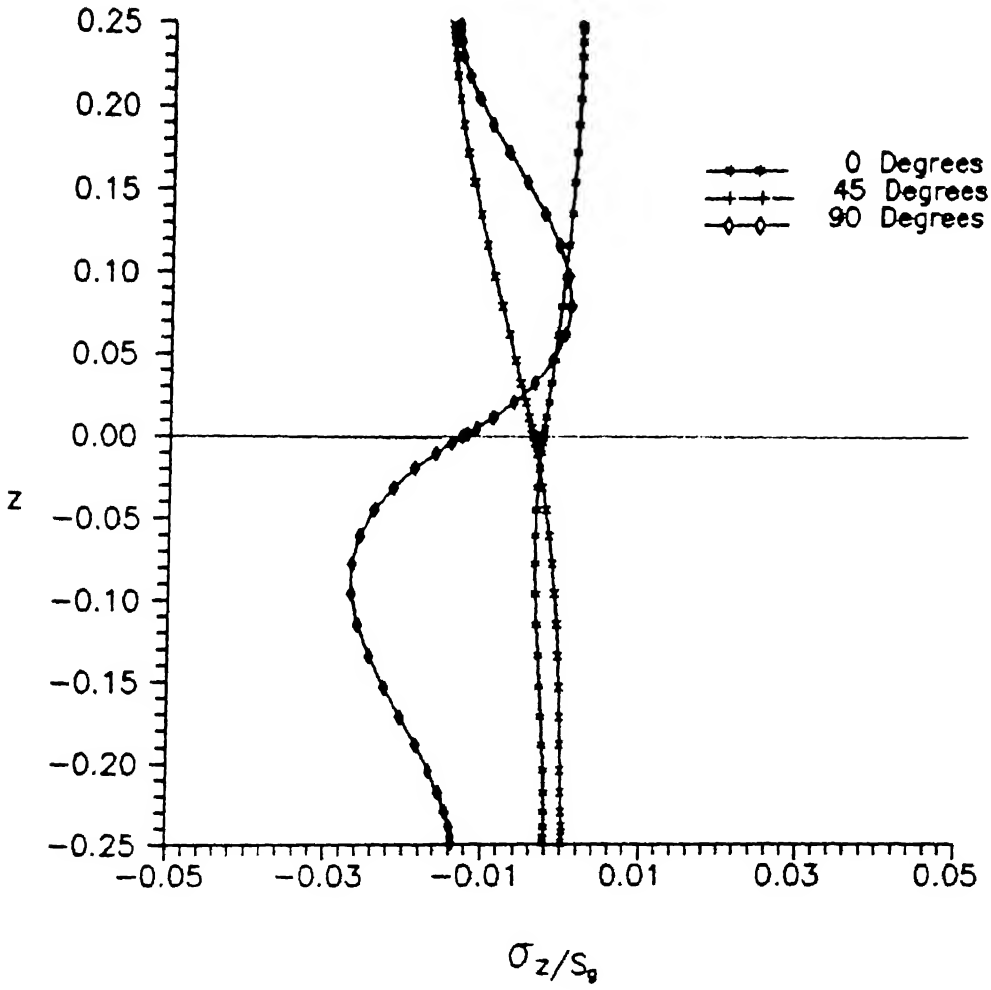

Fig.4.16 σ_z through thickness distribution for 90/0 laminate with circular hole (85 elements)

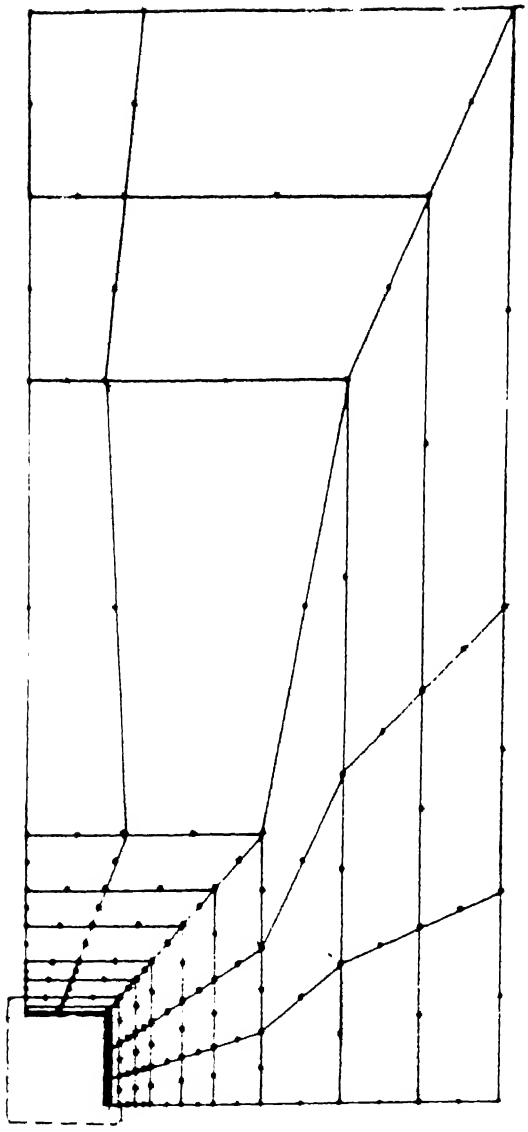

NO. OF ELEMENTS = 85

NO. OF NODES = 300

NO. OF TOTAL DEGREES OF FREEDOM = 2700

R = 5" ; b = 30" ; l = 60

THICKNESS (PLY) = 0.25"

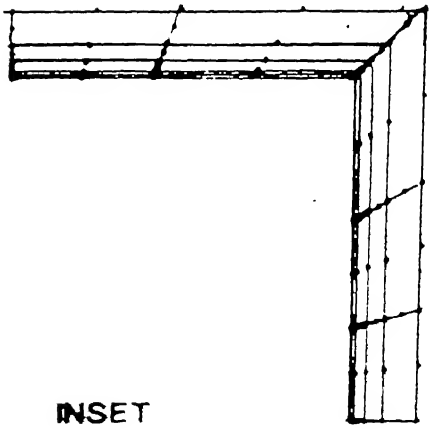

INSET

FIG.4.17. FEM DISCRETIZATION OF LAMINATE PLATE WITH SQUARE HOLE

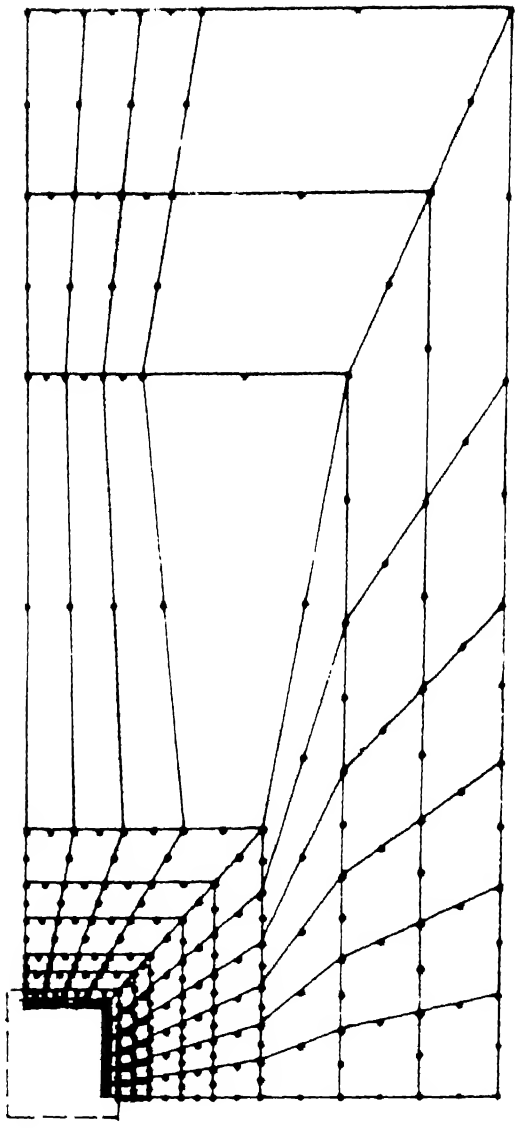

NO. OF ELEMENTS = 170

NO. OF NODES = 565

NO. OF TOTAL DEGREES OF FREEDOM = 5065

R = 5" ; b = 30" ; l = 60"

THICKNESS (PLY) = 0.25"

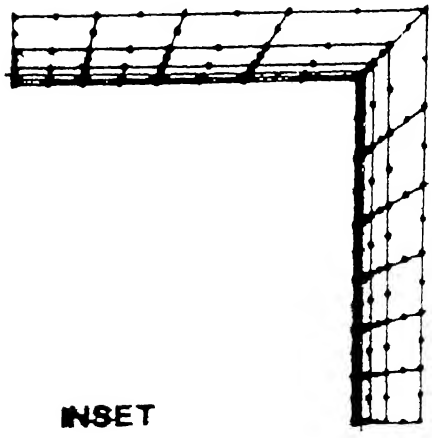

INSET

FIG.4.18. FEM DISCRETIZATION OF LAMINATE PLATE WITH SQUARE HOLE

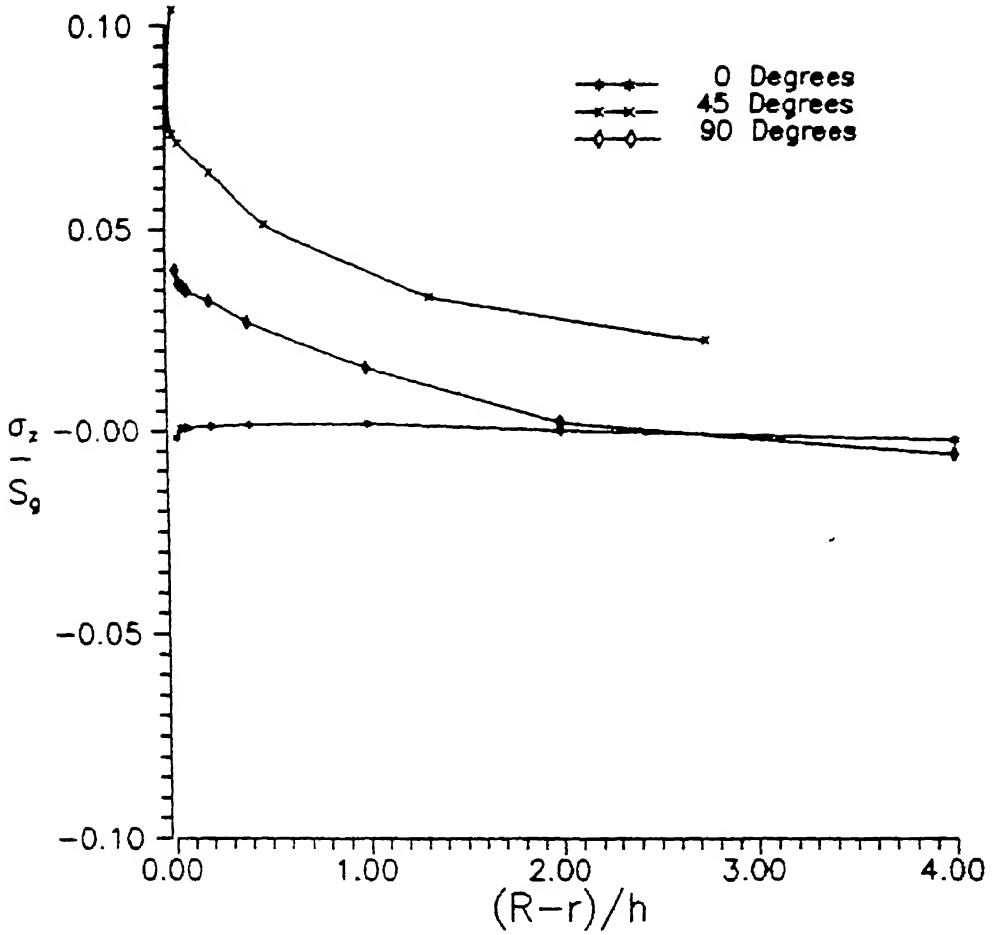

Fig.4.19 σ_z radial distribution for 0/90 laminate with square hole (85 elements)

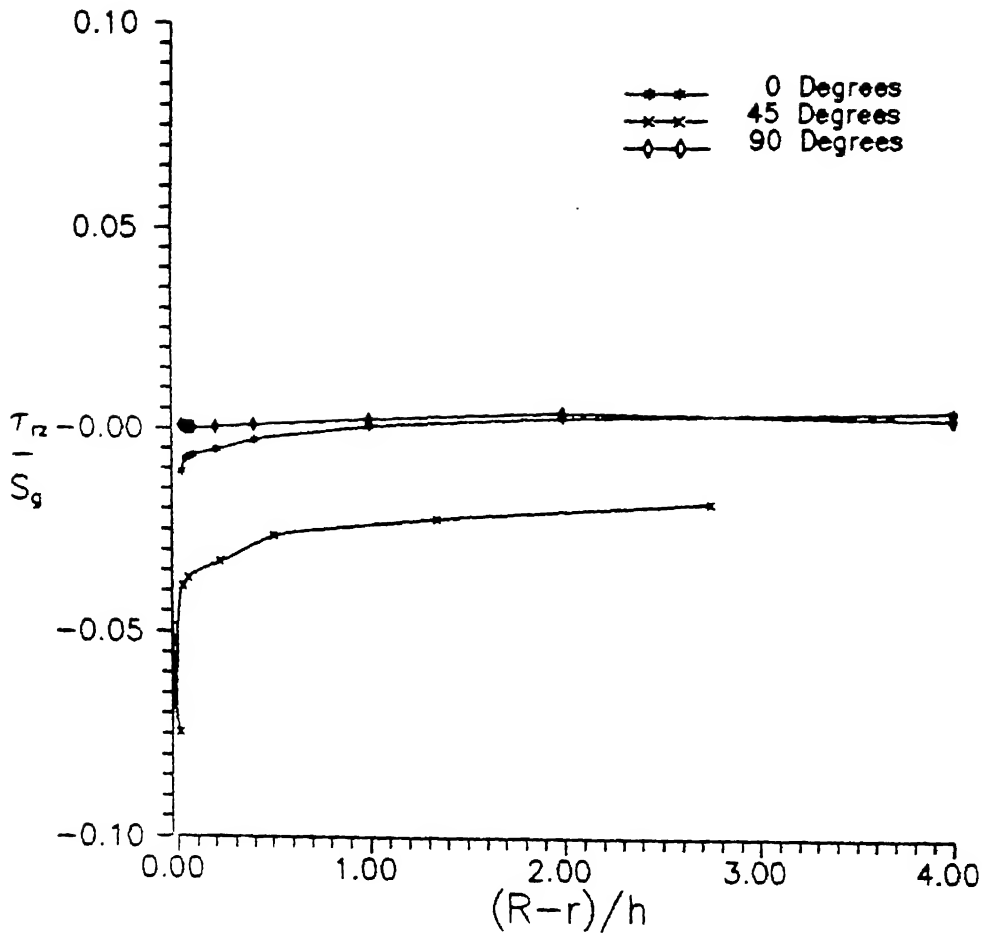

Fig.4.20 τ_{rz} radial distribution for 0/90 laminate with square hole (170 elements)

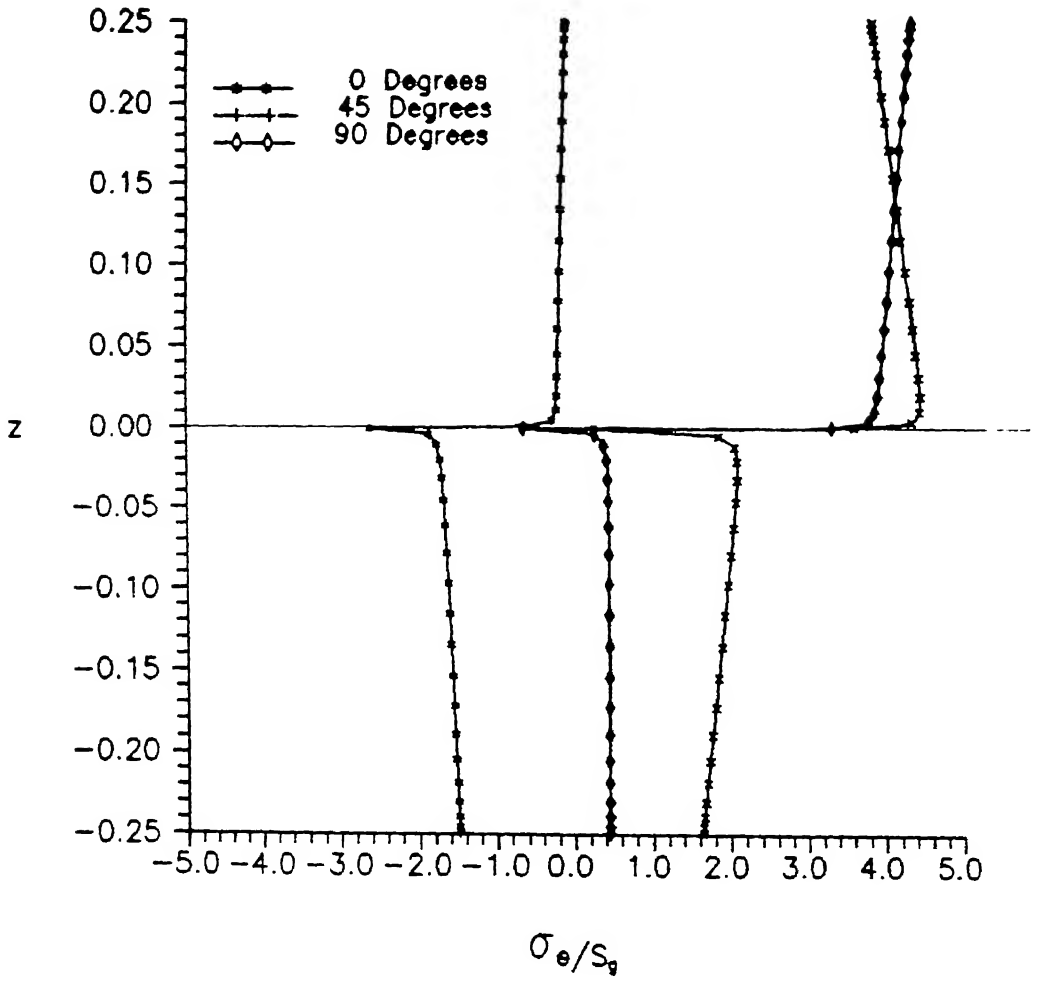

Fig.4.21 σ_{θ} through thickness distribution for 0/90 laminate with square hole (85 elements)

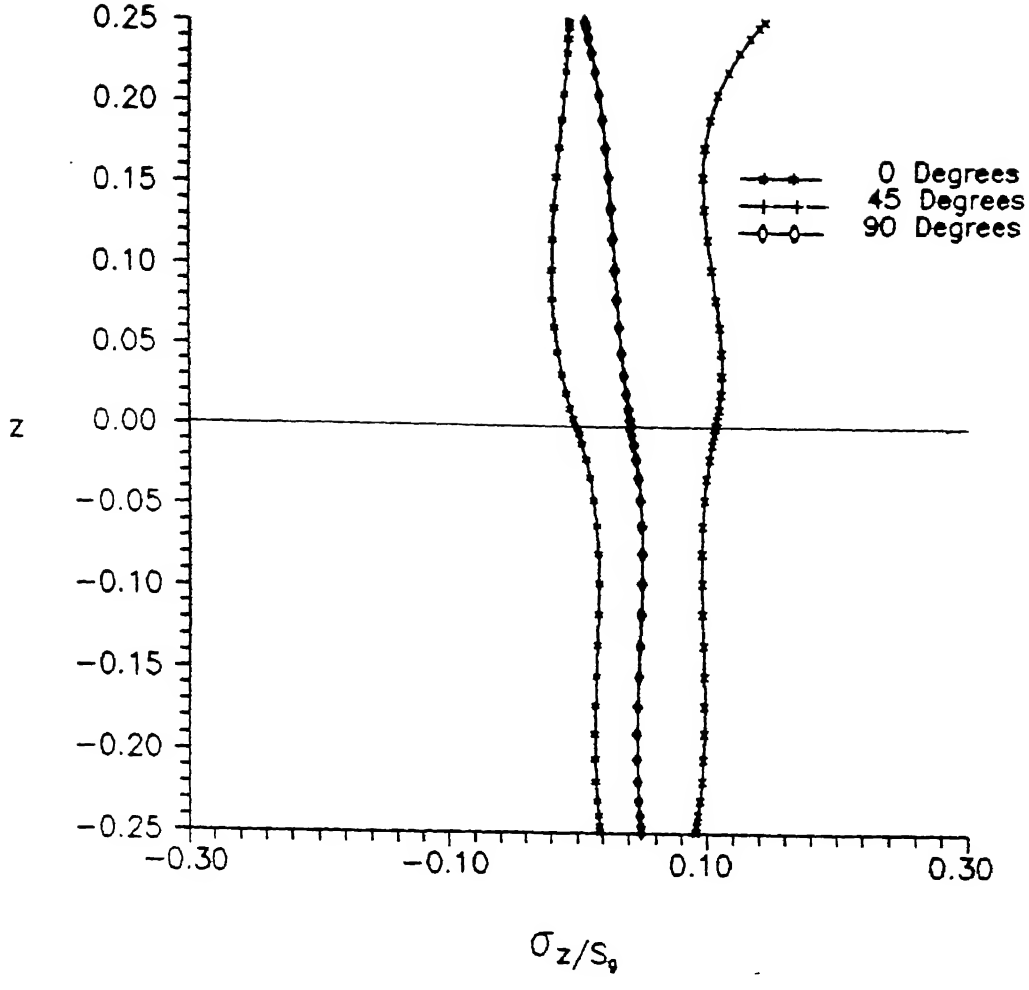

Fig.4.22 σ_z through thickness distribution for 0/90 laminate with square hole (85 elements)

CHAPTER 5

CONCLUSIONS AND SCOPE FOR FURTHER WORK

5.1 Conclusions

The present work deals with the edge effects in symmetric laminated composite plates with a central circular/square hole and subjected to a farfield uniaxial tensile load. Based on the results obtained in the previous chapter, the following conclusions may be arrived at :

1. The singular hybrid finite element method shows a distinct improvement over the nonsingular hybrid method. This tool can be effectively used to study the behaviour of layered composites.

2. For the $[0/90]_S$ configuration, the possibility of delamination exists in the direction perpendicular to the direction of loading, denoted as $\theta = 90^{\circ}$ in the previous discussion, where the transverse normal stress, σ_z has a high tensile value. The presense of high transverse shear stresses, viz. τ_{rz}, in this direction may lead to mixed mode failures.

3. In case of the square hole problem, the magnitudes of these stresses was much higher as compared to the circular hole case, indicating the higher tendancy for delamination.

4. In all the cases, the interlaminar stresses have high magnitudes near the hole boundary and they die down quickly, within a distance of approximately four times the laminate thickness away from the boundary.

3.2 Scope For Future Work

The present work, though satisfactory, has a few shortcomings which,

if overcome, may improve the results by a large extent while using lesser amount of computing time.

1. Instead of the assumption of an axisymmetric case, a complete three-dimensional analysis should be attempted. The angular variation of material properties should be modelled in a better manner during the calculation of the power of singularity.

2. The accurate enforcement of the traction free boundary conditions at the free edge should be made.

3. New shape functions should be tried to achieve exact geometric mapping of the odd shaped elements near the hole boundary.

REFERENCES

Agarwal, B.D. and Brouthman, L.J. "Analysis and performance of fibre composites", John Wiley and Sons, New York (1980)

Altus, E., Ratem, A. and Shmeli, M. "Free edge effect in angle-ply laminates - A new finite difference solution", J. Comps. Mater. , 14, 21-30 (1980)

Bogy, D.B. "Edge-bonded dissimilar orthogonal elastic wedges under normal and shear loading", J. Appl. Mech., 35, 460(1968)

Chahande A. "Application of hybrid finite element method to find interlaminar stresses in composites", M.Tech Thesis, IIT-Kanpur(1989)

Chaudhari, R.A. and Seide, P. "An approximate semi-analytical method for prediction of interlaminar shear stresses in arbitrarily laminated thick plates", Comp. Struct., 25, 627-636(1987)

Hildebrand, F.B. "Advanced calculas for applications", Prentice-Hall Inc., New Jersey

Isakson, G. and Levy, A. "Finite element analysis of interlaminar shear fibrous composites", J. Comps. Mater., 5, 273-276(1971)

Kassapoglou, C. and Lagace, P.A. "An efficient method for calculation of interlaminar stresses in composite materials", ASME J. Appl. Mech., 53, 744-750 (1986)

Lee, J.D. "Three dimensional finite element analysis of layered fiber-reinforced composite material", Comp. Struct., 12, 319-339(1980)

Pagano, N.J. and Pipes, R.B. "The influence of stacking sequence on laminate strength", J. Comps. Mater., 5, 50-57(1971)

Pagano, N.J. "Onthe calculation of interlaminar normal stress in composite laminates", J. Comps. Mater., 8, 65-81(1974)

Pagano, N.J. "Free edghe stress fields in composite laminates", Int. J. of Solids and Struct., 14, 400-406(1978)

Pian, T.N.H. "Hybrid elements", Int. J. for Numer. Methods in Engg., 4, 59-78(1973)

Pipes, R.B. and Pagano, N.J. "Interlaminar stresses in composites under uniform axial extension", J. Comps. Mater., 4, 538-548(1970)

Pipes, R.B. and Daniel, I.M. "Moire analysis of the interlaminar shear edge effect in laminated composites", J. Comps. Mater., 5, 255-259(1971)

Pipes, R.B. and Pagano, N.J. "Interlaminar stresses in composite laminates - An approximate elasticity solution", ASME J. Appl. Mech., 41,. 668-672(1974)

Puppo, A.H. and Evensen, H.A. "Interlaminar shear in laminated composites under generalized plane stress", J. Comps. Mater., 4, 204-220(1970)

Raju, I.S. and Crews, J.H. "Interlaminar stress singularities at a straight free edge in composite laminates", Comp. Struct., 14, 21-28(1981)

Raju, I.S. and Crews, J.H. "Three dimensional analysis of $[0/90]_S$ and $[90/0]_S$ laminates with a central circular hole", Comps. Tech. Review, 4, 116-124(1982)

Rohwer, K. "On the determination of edge stresses in layered composites", Nucl. Engg. and Des., 70, 57-65(1982)

Ryibicki, E.F. "Approximate three dimensional solutions for symmetric laminates under inplane loading", J. Comps. Mater., 5, 354-360(1971)

Spilker, R.L. and Chow, S.C. "Edge effect in symmetric composite laminates: Importance of satisfying the traction-free-edge condition", J. Comps. Mater., 14, 2-20(1980)

Spilker, R.L. and Munir, N.I. "The hybrid stress model for thin plates", Int. J. for Num. Methods in Engg., 15, 1239-1260(1980)

Spilker, R.L. and Munir, N.I. "A Serendipity cubic dispalcement stress

element for thin and moderately thick plates", Int. J. for Num. Methods in Engg., 15, 1261-1278(1980)

Spilker, R.L. "A hybrid stress formulation for thick multilayered laminates", Comps. Struct., 11, 507-514(1980)

Spilker, R.L. "Hybrid stress eight-node element for thin and thick multilayered laminated plates", Int. J. for Num. Methods in Engg., 18, 801-828(1982)

Suresh, N. "Stress analysis of a composite plate with a circular hole-An hybrid FEM approach", M.tech Thesis, IIT-Kanpur(1987)

Tang, S. "Interlaminar stresses of uniformly loaded rectangular composite plates", J. Comps. Mater., 10, 69-78(1976)

Tang, S. "Interlaminar stresses around circular cutouts in composite plates under tension", AIAA Journal, 15, 1631-1637(1977)

Timoshenko, S.P. and Goodier, J.N. "Theory of elasticity", McGraw Hill Co.

Wang, S.S. and Choi, I. "Boundary layer effects in composite laminates : Part-I - Free edge stress singularities", J. of Appl. Mech., 49, 541(1982)

Wang, A.S.D. and Crossman, F.W. "Some new results on edge effects in symmetric composite laminates", J. Comps. Mater., 11, 92-106(1977)

Wang, J.T.S. and Dickson, J.N. "Interlaminar stresses in symmetric composite laminates", J. Comps. Mater., 12, 390-402(1978)

Wang, S.S. and Yuan, F.K. "A singular hjybrid finite element analysis of boundary layer stresses in composite laminates", Int. J. of Solids and Struct., 19, 825-837(1983)

Yamada, Y. and Kumura, H.O. "Finite element analysis of stress and strain singularity eigenstate in inhomogeneous media or composite materials",Hybrid and mixed finiye element method, Atluri, S.N., Gallagher, R.H. and Zienckiewicz, O.C., Eds., John Wiley and Sons Ltd.(1983)

Zienckiewicz, O.C. "The finite element method", Tata McGraw Hill Publishing Co. Ltd. New Delhi, 1977

APPENDIX - A

The 69 β stress assumption is given below :

$$\sigma^i_x = \beta_{17} + [\tfrac{1}{2}(\beta_1 - \beta_{54}) - \beta_{27}]x + \beta_{28}\,y + [\tfrac{1}{4}(\beta_2 - \beta_{55}) - \tfrac{1}{2}\beta_{29}]\,x^2$$

$$+ [\tfrac{1}{2}(\beta_3 - \beta_{56}) - 2\,\beta_{30}]xy + \beta_{19}\,y^2 + [\tfrac{1}{6}(\beta_4 - \beta_{57}) - \tfrac{1}{3}\beta_{32}]\,x^3$$

$$+ [\tfrac{1}{4}(\beta_5 - \beta_{58}) - \beta_{33}]\,x^2y + [\tfrac{1}{2}(\beta_6 - \beta_{59}) - 3\,\beta_{34}]\,xy^2 + \beta_{19}\,y^3$$

$$+ \tau\Big\{\beta_{35} + \beta_{36}\,x + \beta_{37}\,y + \beta_{38}\,x^2 + \beta_{39}\,xy + \beta_{40}\,y^2$$

$$+ [-\tfrac{3}{4}(\beta_{68} - \beta_{15} + \beta_5 + \beta_{58} + 2\,\beta_{12} + 2\,\beta_{65})\,x^2y + \beta_{41}\,xy^2\Big\}$$

$$\sigma^i_y = \beta_{21} + \beta_{22}\,x + [\tfrac{1}{2}(\beta_7 - \beta_{51}) - \beta_{26}]\,y + \beta_{23}\,x^2 + [\tfrac{1}{2}(\beta_8 - \beta_{61}) - 2\,\beta_{28}]\,xy$$

$$+ [\tfrac{1}{4}(\beta_9 - \beta_{62}) - \tfrac{1}{2}\beta_{29}]\,y^2 + \beta_{24}\,x^3 + [\tfrac{1}{2}(\beta_{10} - \beta_{63}) - 3\,\beta_{31}]\,x^2y$$

$$+ [\tfrac{1}{4}(\beta_{11} - \beta_{64}) - \beta_{32}]\,xy^2 + [\tfrac{1}{6}(\beta_{12} - \beta_{65}) - \tfrac{1}{3}\beta_{33}]\,y^3$$

$$+ \tau\Big\{\beta_{42} + \beta_{43}\,x + \beta_{44}\,y + \beta_{45}\,x^2 + \beta_{46}\,xy + \beta_{47}\,y^2 + \beta_{48}\,x^2y$$

$$+ [-\tfrac{3}{4}(\beta_{67} - \beta_{14} + 2\,\beta_4 + 2\,\beta_{57} + \beta_{11} + \beta_{64})\,xy^2\Big\}$$

$$\sigma^{i}_{xy} = \beta_{25} + \beta_{26}\,x + \beta_{27}\,y + \beta_{28}\,x^2 + \beta_{29}\,xy + \beta_{30}\,y^2 + \beta_{31}\,x^3 + \beta_{32}\,x^2y$$

$$+ \beta_{33}\,xy^2 + \beta_{34}\,y^3 + \tau\left\{ \beta_{49} + \beta_{50}\,x + \beta_{51}\,y + \beta_{52}\,x^2 + \left[-\tfrac{3}{4}\left(\beta_{66} \right.\right.\right.$$

$$\left.\left.\left. - \beta_{13} + \beta_{2} + \beta_{55} + \beta_{9} + \beta_{62} \right) - \left(\beta_{38} + \beta_{37} \right) \right] xy + \beta_{53}\,y^2 \right\}$$

$$\sigma^{i}_{yz} = \bar{t}_i \left\{ \tfrac{1}{2}\,(1 - \tau)\,(\beta_7 + \beta_8\,x + \beta_{10}\,x^2 + \beta_{12}\,y^2) + \tfrac{1}{8}(1 - \tau)(1 - 3\,\tau)\beta_9\,y \right.$$

$$+ \tfrac{1}{4}(1 - \tau)(-1 - 3\,\tau)\,\beta_{11}\,xy + \tfrac{1}{2}(1 + \tau)\,(\beta_{60} + \beta_{61}\,x + \beta_{62}\,x^2 + \beta_{65}\,y^2)$$

$$+ \tfrac{1}{8}(1 + \tau)(1 + 3\,\tau)\,\beta_{62}\,y + \tfrac{1}{4}(1 + \tau)(-1 + 3\,\tau)\,\beta_{64}\,xy$$

$$\left. + \tfrac{1}{4}(1 - \tau^2) \left\{ (\beta_{44} + \beta_{50}) + (\beta_{45} + 2\,\beta_{52})\,x + \left[-\tfrac{3}{4}\,(\beta_{66} - \beta_{13} + \beta_{2} \right.\right.\right.$$

$$\left.\left.\left. + \beta_{55}) + (\beta_{47} - \beta_{38}) \right] y + \beta_{48}\,x^2 + \left[-\tfrac{3}{2}\,(\beta_{67} - \beta_{14}) - 3\,(\beta_{4} + \beta_{57}) \right] xy \right\} \right\}$$

$$\sigma^{i}_{xz} = \bar{t}_i \left\{ \tfrac{1}{2}\,(1 - \tau)\,(\beta_1 + \beta_9\,y + \beta_4\,x^2 + \beta_6\,y^2) + \tfrac{1}{8}(1 - \tau)(1 - 3\,\tau)\,\beta_2\,y \right.$$

$$+ \tfrac{1}{4}(1 - \tau)(-1 - 3\,\tau)\,\beta_5\,xy + \tfrac{1}{2}(1 + \tau)\,(\beta_{54} + \beta_{56}\,x + \beta_{57}\,x^2 + \beta_{59}\,y^2)$$

$$+ \tfrac{1}{8}(1 + \tau)(1 + 3\,\tau)\,\beta_{55}\,x + \tfrac{1}{4}(1 + \tau)(-1 + 3\,\tau)\,\beta_{58}\,xy$$

$$\left. + \tfrac{1}{2}(1 - \tau^2) \left\{ (\beta_{36} + \beta_{51}) + \left[-\tfrac{3}{4}\,(\beta_{66} - \beta_{13} + \beta_{9} + \beta_{62}) + (\beta_{38} \right.\right.\right.$$

$$- \beta_{47})] x + (\beta_{39} + 2 \beta_{53}) y + [-\tfrac{3}{2} (\beta_{68} - \beta_{15}) - 3 (\beta_{12} + \beta_{65})] xy$$

$$+ \beta_{41} y^2 \} \}$$

$$\sigma^i_z = \bar{t}_i^2 \left\{ \tfrac{1}{4} (1 - \tau)^2 (2 + \tau) (\beta_{13} + \beta_{14} x + \beta_{15} y) + \tfrac{1}{4} (1 + \tau)^2 (2 - \tau) \right.$$

$$(\beta_{66} + \beta_{67} x + \beta_{68} y) - \tfrac{1}{4} (1 - \tau)^2 (1 + \tau) ((\beta_2 + \beta_9) + (2 \beta_4 + \beta_{11}) x$$

$$+ (\beta_5 + 2 \beta_{12}) y + \tfrac{1}{4} (1 - \tau) (1 + \tau)^2 [(\beta_{55} + \beta_{62}) + (2 \beta_{57} + \beta_{64}) x$$

$$\left. + (\beta_{58} + 2 \beta_{65}) y] \right\}$$

APPENDIX - B

The standard bi-quadratic serendipity shape functions used for 8-noded quadrilateral elements are :

$$N_1 (\xi , \eta) = (1 - \xi) (1 - \eta) (-1 - \xi - \eta) / 4$$

$$N_2 (\xi , \eta) = (1 - \xi^2) (1 - \eta) / 2$$

$$N_3 (\xi , \eta) = (1 + \xi) (1 - \eta) (-1 + \xi - \eta) / 4$$

$$N_4 (\xi , \eta) = (1 + \xi) (1 - \eta^2) / 2$$

$$N_5 (\xi , \eta) = (1 + \xi) (1 + \eta) (-1 + \xi + \eta) / 4$$

$$N_6 (\xi , \eta) = (1 - \xi^2) (1 + \eta) / 2$$

$$N_7 (\xi , \eta) = (1 - \xi) (1 + \eta) (-1 - \xi + \eta) / 4$$

$$N_8 (\xi , \eta) = (1 - \xi) (1 + \eta^2) / 2$$